o-toluidine and from 6.2% ± 0.3% to 2.6% ± 0.2% for 2,6-xylidine) and slightly decreased by incubation with an anti-CYP3A4 antibody (to 16.9% ± 0.5% for *o*-toluidine and to 4.3% ± 0.3% for 2,6-xylidine). Incubation with an anti-CYP1A2 antibody also slightly decreased 2,6-xylidine–induced Met-Hb formation (to 5.0% ± 0.5%).

To investigate the contribution of CYP3A4 to prilocaine- and lidocaine-induced Met-Hb formation in the absence of hydrolysis, inhibition analyses were performed using anti-P450 antibodies (Fig. 7B). When 100 μM DFP was used to inhibit CES enzyme activity, incubation with an anti-CYP3A4 antibody substantially decreased prilocaine- and lidocaine-induced Met-Hb formation (from 5.7% ± 0.4% to 0.6% ± 0.3% for prilocaine and from 3.4% ± 0.4% to 0.7% ± 0.2% for lidocaine).

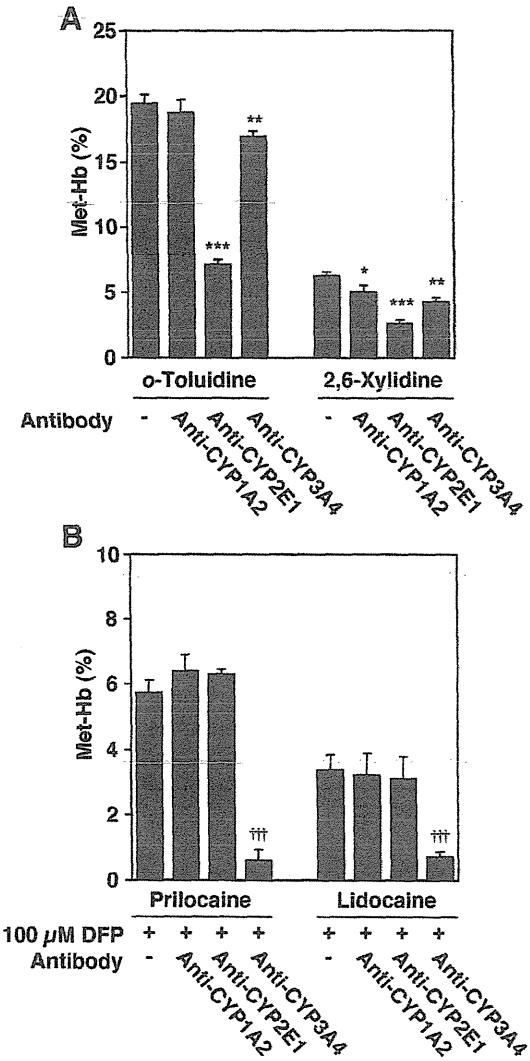

Fig. 7. Inhibitory effects of anti-human CYP1A2, CYP2E1, and CYP3A4 antibodies on *o*-toluidine–, 2,6-xylidine–, prilocaine-, and lidocaine-induced Met-Hb formations in HLM. HLM (0.5 mg/ml) were incubated with 1 mM *o*-toluidine, 1 mM 2,6-xylidine (A), 10 mM prilocaine, or 10 mM lidocaine (in the presence of 100 μM DFP) (B), an NADPH-GS, mouse red blood cells, and each P450 antibody. Met-Hb formation in the absence of antibody was 19.5% ± 0.6% (*o*-toluidine) and 6.2% ± 0.3% (2,6-xylidine), and Met-Hb formation in the absence of antibody but in the presence of DFP was 5.7% ± 0.4% (prilocaine) and 3.4% ± 0.4% (lidocaine). The incubation time was 120 minutes (prilocaine and lidocaine) and 60 minutes (*o*-toluidine and 2,6-xylidine). Each column represents the mean ± S.D. of triplicate determinations. Differences compared to control with no antibody were considered significant at $^{*}P < 0.05$; $^{**}P < 0.005$; and $^{***}P$ or $\dagger\dagger\dagger P < 0.001$.

Met-Hb Formation in the Presence of the Hydroxylated Metabolites of *o*-Toluidine and 2,6-Xylidine. 4-Hydroxy-*o*-toluidine, 6-hydroxy-*o*-toluidine, or 4-hydroxy-2,6-xylidine has been detected in human urine after the administration of prilocaine or lidocaine (Hjelm et al., 1972; Keenaghan and Boyes, 1972). To investigate whether these metabolites could induce Met-Hb formation, in vitro analyses were performed. 4-Hydroxy-*o*-toluidine–,6-hydroxy-*o*-toluidine–, and 4-hydroxy-2,6-xylidine–induced Met-Hb formation were markedly increased, in both the presence and the absence of an NADPH-GS (Fig. 8). A higher degree of Met-Hb formation was detected in the presence of these metabolites than in the presence of *o*-toluidine and 2,6-xylidine. Thus, it was suggested that these hydroxylated metabolites of *o*-toluidine and 2,6-xylidine were one of the causative factors underlying prilocaine- and lidocaine-induced methemoglobinemia.

Formation of the Hydroxylated Metabolites of *o*-Toluidine and 2,6-Xylidine in HLM. Because the hydroxylated metabolites of *o*-toluidine and 2,6-xylidine could induce Met-Hb formation, we investigated whether HLM could catalyze the hydroxylation of *o*-toluidine and 2,6-xylidine (Fig. 9, A and B). Data for these hydroxylase activities in HLM followed Michaelis-Menten kinetics. The K_m and V_{max} values for 4-hydroxylation of *o*-toluidine in HLM were 50.2 ± 2.8 μM and 0.61 ± 0.03 nmol/min/mg protein, respectively, resulting in a CL_{int} value of 12.2 ± 0.2 μl/min/mg protein. The K_m and V_{max} values for 6-hydrolxylation of *o*-toluidine in HLM were 70.3 ± 6.2 μM and 0.05 ± 0.00 nmol/min/mg protein, respectively, resulting in a CL_{int} value of 0.7 ± 0.1 μl/min/mg protein (Table 2). Thus, the CL_{int} value for 4-hydroxylation of *o*-toluidine in HLM was

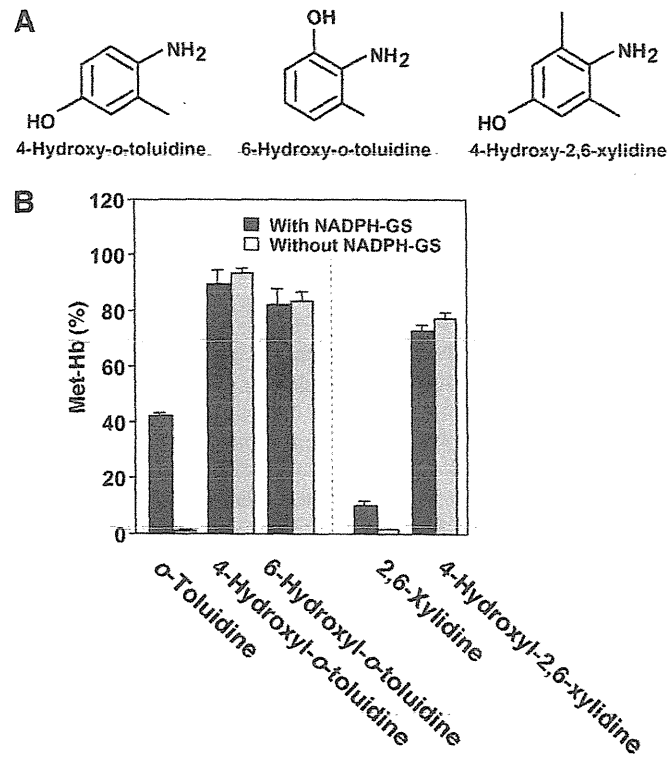

Fig. 8. (A) Chemical structures of 4-hydroxy-*o*-toluidine, 6-hydroxy-*o*-toluidine, and 6-hydroxy-2,6-xylidine. (B) Met-Hb formation induced by the hydroxylated metabolites of *o*-toluidine and 2,6-xylidine. *o*-Toluidine, 4-hydroxy-*o*-toluidine, 6-hydroxy-*o*-toluidine, 2,6-xylidine, or 4-hydroxy-2,6-xylidine (1 mM) was incubated with HLM (1.0 mg/ml) and mouse red blood cells in the presence or absence of an NADPH-GS for 60 minutes. Each column represents the mean ± S.D. of triplicate determinations.

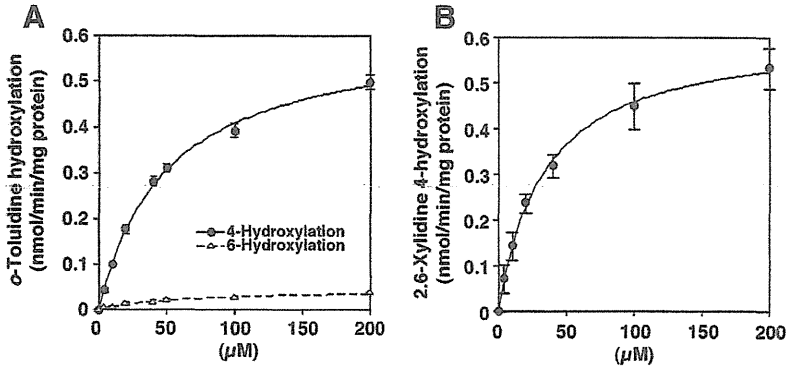

Fig. 9. Kinetic analyses of *o*-toluidine and 2,6-xylidine hydroxylase activities in HLM. HLM (0.4 mg/ml) was incubated with *o*-toluidine (A) and 2,6-xylidine (B) for 30 minutes. *o*-Toluidine and 2,6-xylidine hydroxylase activities were measured by quantitative analyses of 4- or 6-hydroxyl-*o*-toluidine and 4-hydroxy-2,6-xylidine, respectively, using HPLC. Each data point represents the mean ± S.D. of triplicate determinations.

shown to be 18-fold higher than that for 6-hydroxylation. The K_m and V_{max} values for 4-hydroxylation of 2,6-xylidine in HLM were 34.1 ± 5.1 μM and 0.61 ± 0.04 nmol/min/mg protein, respectively, resulting in a CL_{int} value of 18.3 ± 3.4 μl/min/mg protein. These results indicate that *o*-toluidine and 2,6-xylidine were efficiently metabolized to their hydroxylated forms in HLM.

Inhibition Analyses of *o*-Toluidine and 2,6-Xylidine Hydroxylase Activities in the Presence of Anti-P450 Antibodies. To further investigate the contributions of CYP1A2, CYP2E1, and CYP3A4 to *o*-toluidine and 2,6-xylidine hydroxylation in HLM, inhibition analyses were performed using anti-P450 antibodies (Fig. 10). *o*-Toluidine 4- and 6-hydroxylase activities were markedly decreased (percentage of control: 35.4% ± 1.6% for *o*-toluidine 4-hydroxylation and 47.1% ± 2.3% for *o*-toluidine 6-hydroxylation) by incubation with an anti-CYP2E1 antibody. 2,6-Xylidine 4-hydroxylase activity was also markedly decreased by incubation with an anti-CYP2E1 (percentage of control: 25.6% ± 0.9%) and slightly decreased by incubation with an anti-CYP3A4 antibody (percentage of control: 92.9% ± 0.3%). Thus, it was suggested that CYP2E1 could mainly catalyze *o*-toluidine and 2,6-xylidine hydroxylations, leading to Met-Hb formation.

Prilocaine- and Lidocaine-Induced Met-Hb Formation in Human Red Blood Cells. In the aforementioned Met-Hb formation analyses, mouse red blood cells were used. To assess species-specific differences in Met-Hb formation between mice and humans, an analysis using human red blood cells that were obtained from 5 individuals was conducted as follows: prilocaine or lidocaine (10 mM) was incubated with HLM, an NADPH-GS, and individual human red blood cells that had been obtained from the five healthy donors. The levels of Met-Hb formation in the absence of prilocaine or lidocaine were 0.6–1.5% (mean, 1.1%). High Met-Hb formation was observed after incubation with both prilocaine and lidocaine [prilocaine: mean, 34.8% (26.8–41.5%); lidocaine: mean, 9.9% (9.0–11.3%)], but the formation of Met-Hb was significantly decreased by incubation with 100 μM DFP [prilocaine: mean, 7.6% (6.8–8.6%); lidocaine: mean, 6.4% (5.1–7.4%)] (Fig. 11). This result was similar to that obtained using mouse red blood cells (Fig. 4). These results indicate the comparable Met-Hb formation sensitivity between human and mouse red blood cells.

TABLE 2

Kinetic parameters of the hydroxylase activities of *o*-toluidine and 2,6-xylidine

HLM: 0.4 mg/ml. Data are the mean ± S.D. of triplicate determinations.

Hydroxylase Reaction	K_m	V_{max}	CL_{int}
	μM	*nmol/min/mg protein*	*μl/min/mg protein*
o-Toluidine			
4-Hydroxylation	50.2 ± 2.8	0.61 ± 0.03	12.2 ± 0.2
6-Hydroxylation	70.3 ± 6.2	0.05 ± 0.00	0.7 ± 0.1
2,6-Xylidine			
4-Hydroxylation	34.1 ± 5.1	0.61 ± 0.04	18.3 ± 3.4

Discussion

Prilocaine and lidocaine are typical amide-type local anesthetics that carry the risk of a serious adverse reaction known as methemoglobinemia (Maimo and Redick, 2004). Prilocaine and lidocaine are hydrolytically metabolized to the aromatic amines *o*-toluidine and 2,6-xylidine, respectively. Although these metabolites were suspected to be causes of prilocaine- and lidocaine-induced methemoglobinemia (Neuhaeuser et al., 2008), the enzymes responsible for Met-Hb formation remained to be characterized. In the present study, we found that metabolic activation by human CES, CYP2E1, and CYP3A4 was involved in prilocaine- and lidocaine-induced methemoglobinemia.

We demonstrated that prilocaine was hydrolyzed by CES1A and CES2, whereas lidocaine was specifically hydrolyzed by CES1A (Fig. 1), and that hydrolysis reactions that were catalyzed by CES enzymes enhanced prilocaine- and lidocaine-induced Met-Hb formation (Figs. 2 and 4). Because prilocaine and lidocaine hydrolase activities were detected in HLM, but not in human plasma where cholinesterases and paraoxonases are expressed (unpublished data), these enzymes could be excluded from the candidate enzymes catalyzing their hydrolysis. Recombinant human AADAC showed no activity (Fig. 1; Table 1). Moreover, prilocaine and lidocaine hydrolase activities at 1 mM were completely inhibited by 100 μM DFP and BNPP (unpublished data), which are potent CES inhibitors (Watanabe et al., 2009). Collectively, these results suggest that CES enzymes are major enzymes that are responsible for the hydrolysis of prilocaine and lidocaine.

Met-Hb formation after the incubation of the parent compounds (prilocaine and lidocaine) with HLM was lower than that after incubation of their hydrolyzed metabolites (*o*-toluidine and 2,6-xylidine) (Fig. 2). Prilocaine- and lidocaine-induced Met-Hb formation was significantly decreased by DFP and BNPP (Fig. 4), indicating that CES enzymes may be involved in the prilocaine- and lidocaine-induced Met-Hb formation. When metabolic efficiency was analyzed, prilocaine was shown to be more efficiently hydrolyzed in HLM than was lidocaine (Fig. 1, A and B). Furthermore, prilocaine- and *o*-toluidine–induced Met-Hb formation was higher than that induced by incubating lidocaine and 2,6-xylidine (Fig. 2, A and B). These results support the previous report (Guay, 2009), which indicates that the number of prilocaine-related methemoglobinemia episodes is higher than that of lidocaine-related methemoglobinemia.

We considered the possibility that hydrolysis may not be the sole cause of prilocaine- and lidocaine-induced methemoglobinemia, because Met-Hb formation was not completely inhibited by DFP and BNPP.

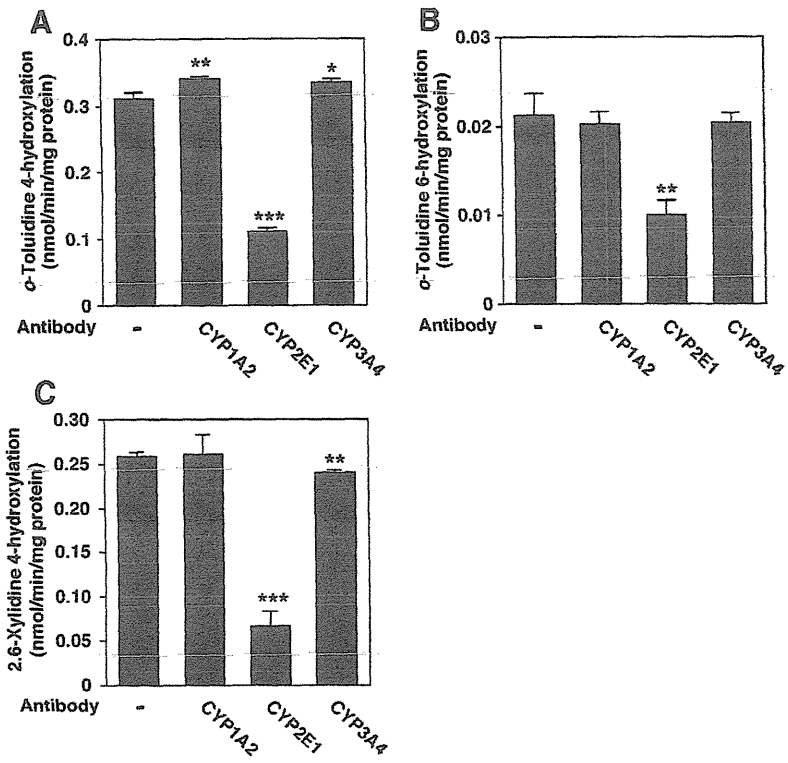

Fig. 10. Inhibitory effects of anti-human CYP1A2, CYP2E1, and CYP3A4 antibodies on *o*-toluidine- or 2,6-xylidine hydroxylation in HLM. HLM (0.4 mg/ml) was incubated with 50 μM *o*-toluidine or 30 μM 2,6-xylidine, an NADPH-GS, and each P450 antibody for 30 minutes. The control activities for *o*-toluidine-4-hydroxylation (A), *o*-toluidine-6-hydroxylation (B), and 2,6-xylidine-4-hydroxylation (C) were 0.31 ± 0.01, 0.02 ± 0.00, and 0.26 ± 0.00 nmol/min/mg protein, respectively. Each column represents the mean ± S.D. of triplicate determinations. Differences compared to control with no antibody were considered significant at $^{*}P < 0.05$; $^{**}P < 0.005$; and $^{***}P < 0.001$.

Supporting this assumption, we observed that metabolism by P450 enzymes was also required for prilocaine- and lidocaine-induced Met-Hb formation in the presence and absence of the hydrolysis reaction (Figs. 2, 3, and 5–7). Human P450 enzymes, which are major NADPH-dependent enzymes, account for ~75% of the metabolism of clinical drugs (Guengerich, 2008). In the absence of an NADPH-GS, Met-Hb formation after incubation with prilocaine, lidocaine, and their hydrolyzed metabolites was not increased (Fig. 2B). In fact, we demonstrated that Met-Hb formation was increased by CYP3A4 (prilocaine and lidocaine) by using recombinant P450 enzymes in the absence of the hydrolysis reaction (Fig. 5). The formation of Met-Hb after incubation with the hydrolyzed metabolites was indeed increased by CYP1A2, CYP2E1, and CYP3A4 (*o*-toluidine) or CYP2E1 (2,6-xylidine) (Fig. 3). When we accounted for the levels of each P450 enzyme in HLM, CYP2E1 appeared to contribute highly to the formations of Met-Hb after incubation with the hydrolyzed metabolites (Fig. 6). These data were consistent with those obtained in the analyses that were conducted in the presence of anti-P450 antibodies (Fig. 7A). Met-Hb formation in the presence of HLM was similar to the sum of Met-Hb formation by each of the individual P450 expression systems (Fig. 6), indicating that these P450 enzymes may be responsible for Met-Hb formation in the presence of prilocaine, lidocaine, *o*-toluidine, or 2,6-xylidine in the presence and absence of the hydrolysis reaction. Collectively, our data indicate that two metabolic pathways, the hydrolysis pathway, which is catalyzed by CES enzymes and CYP2E1, and the nonhydrolysis pathway, which is catalyzed by CYP3A4, may be involved in prilocaine- and lidocaine-induced methemoglobinemia (Fig. 12).

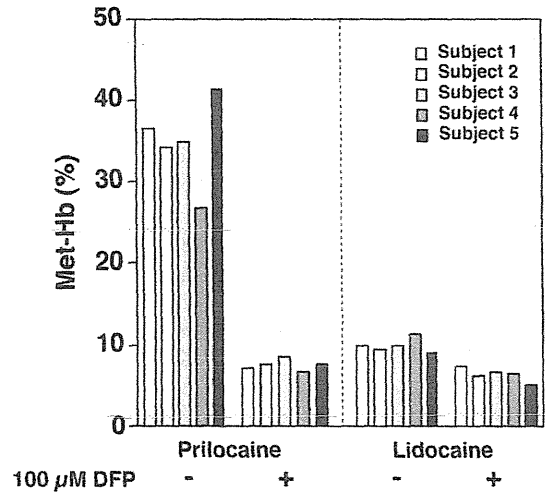

Fig. 11. Prilocaine- and lidocaine-induced Met-Hb formation after incubation with human red blood cells in the absence or presence of 100 μM DFP. HLM (1.0 mg/ml) was incubated for 120 minutes with prilocaine or lidocaine (10 mM), an NADPH-GS, and human red blood cells that had been obtained from five healthy individuals.

By comparing the decreased levels of Met-Hb after incubation with DFP to the residual formation of Met-Hb (Fig. 4), the contributions of the hydrolytic and nonhydrolytic metabolic pathways to prilocaine- and lidocaine-induced Met-Hb formation in HLM can be roughly predicted. The decreases in prilocaine- and lidocaine-induced Met-Hb formation were 2.16- and 0.82-fold greater, respectively, than the residual formation of Met-Hb. Thus, the hydrolysis of prilocaine by CES enzymes highly contributed to prilocaine-induced formation, whereas the hydrolytic and nonhydrolytic pathways of lidocaine seemed to contribute equally to Met-Hb formation.

Methemoglobinemia is reported to be induced by certain types of clinically used drugs, including the analgesic antipyretic phenacetin, the antileprosy drug dapsone, and the antibiotic sulfamethoxazole (Reilly et al., 1999; Ganesan et al., 2010; Kobayashi et al., 2012), which all possess an aromatic amine moiety. *N*-Hydroxylamines, which are *N*-hydroxylated metabolites of aromatic amines, were suspected to be a cause of aromatic amine-induced methemoglobinemia (Spooren and

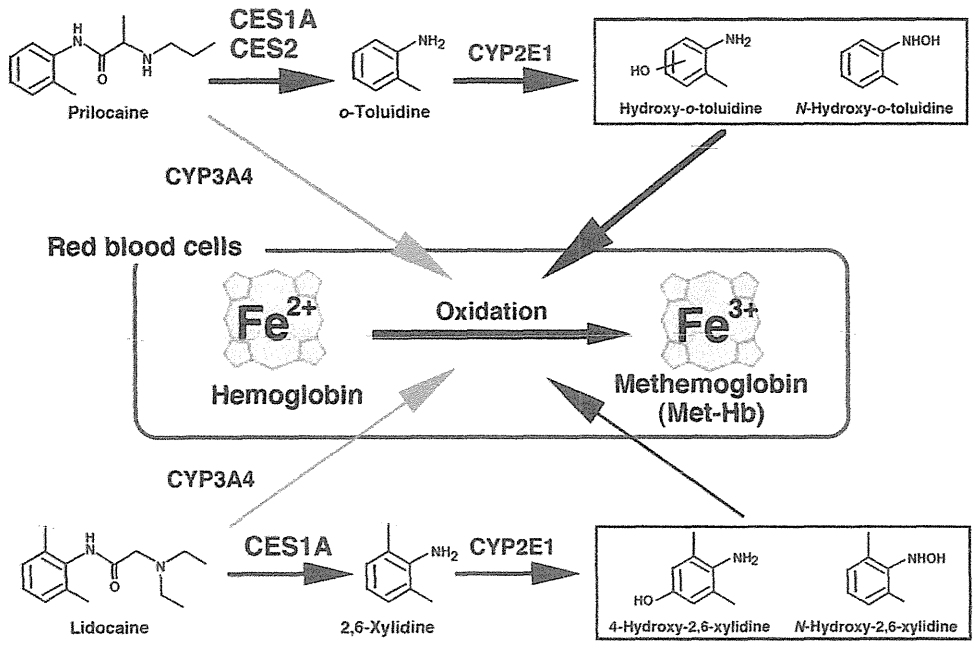

Fig. 12. Mechanisms suggested to underlie prilocaine- and lidocaine-induced Met-Hb formation. Two metabolic pathways are proposed: the hydrolysis pathway, which is mediated by CES and CYP2E1, and the nonhydrolysis pathway, which is mediated by CYP3A4.

Evelo, 2000). For instance, in vitro experimental data indicate that dapsone-hydroxylamine, which is an *N*-hydroxylated metabolite of dapsone that is catalyzed by CYP2C19, CYP2E1, and CYP3A4, may cause dapsone-induced methemoglobinemia (Reilly et al., 1999). Therefore, *N*-hydroxyl-*o*-toluidine and *N*-hydroxyl-2,6-xylidine, which are *N*-hydroxylated metabolites of *o*-toluidine and 2,6-xylidine, respectively, may cause Met-Hb formation after exposure to *o*-toluidine and 2,6-xylidine. Because *N*-hydroxylamines are generally unstable (Fuller, 1978), *N*-hydroxyl-*o*-toluidine and *N*-hydroxyl-2,6-xylidine could not be obtained. 4-Hydroxy-*o*-toluidine and 6-hydroxy-*o*-toluidine or 4-hydroxy-2,6-xylidine (Fig. 8A) have been detected in human urine after the administration of prilocaine or lidocaine, respectively (Hjelm et al., 1972; Keenaghan and Boyes, 1972). We also confirmed that *o*-toluidine and 2,6-xylidine were converted to the hydroxylated metabolites 4- and 6-hydroxy-*o*-toluidine or 4-hydroxy-2,6-xylidine in HLM (Fig. 9) and that hydroxylation of *o*-toluidin and 2,6-xylidine was mainly catalyzed by CYP2E1 (Fig. 10). These hydroxylated metabolites could efficiently induce Met-Hb formation in the absence of an NADPH-GS (Fig. 8B), suggesting that 4- and 6-hydroxy-*o*-toluidine or 4-hydroxy-2,6-xylidine may also cause Met-Hb formation after exposure to *o*-toluidine and 2,6-xylidine, respectively. Although *o*-toluidine more efficiently induced Met-Hb formation than did 2,6-xylidine (Fig. 2), the metabolic efficiency of *o*-toluidine 4-hydroxylation was shown to be lower than that of 2,6-xylidine 4-hydroxylation (Table 2). This discrepancy may be accounted for by the *N*-hydroxylated metabolites. Because we could not compare the induction potencies of Met-Hb formation between the *N*-hydroxylated metabolites and the other hydroxylated metabolites, the metabolite that contributed to Met-Hb formation to the greatest degree could not be determined.

As shown in Figs. 6, C and D, and 7B, CYP3A4 may be involved in prilocaine- and lidocaine-induced Met-Hb formation in the absence of the hydrolysis pathway. Lidocaine is known to be metabolized to monoethylglycinexylidide by CYP3A4, but we confirmed that little Met-Hb was formed after incubation with monoethylglycinexylidide (Supplemental Fig. 1). In addition, lidocaine is metabolized to 3-hydroxylidocaine, but this metabolite was excluded as a potential cause of Met-Hb formation, because it is formed by CYP1A2 and CYP3A4 (Wang et al., 2000). P450 enzymes have not been previously reported to participate in the metabolism of prilocaine. It will be worthwhile to identify the metabolites of prilocaine and lidocaine that cause methemoglobinemia and are catalyzed by CYP3A4 in the near future.

An in vitro assay to determine Met-Hb formation used human red blood cells that had been obtained from five individuals, resulting in comparable sensitivity for Met-Hb formation between human and mouse red blood cells (Figs. 4 and 11). Vasters et al. (2006) reported that interindividual differences in the Met-Hb levels (17.1-fold) varied by more than the variation observed after different dosages of prilocaine (1.4-fold). Neuhaeuser et al. (2008) reported that there were large interindividual variations in Met-Hb levels (8.8-fold) despite the similar dosages of lidocaine that had been administered to patients. In this study, no interindividual variability in Met-Hb formation was observed in individual red blood cells that were treated with prilocaine and lidocaine (Fig. 11). Therefore, we suggest that interindividual variations in Met-Hb formation after treatment with prilocaine and lidocaine were not attributable to hemoglobin in red blood cells per se, but rather to the metabolic potencies of enzymes, CES, and P450s, and Met-Hb reductases.

In conclusion, the present study clarified that two metabolic pathways, the hydrolysis pathway, which means the hydroxylation by CYP2E1 after the hydrolysis by CES(s), and the nonhydrolysis pathway, which is catalyzed by CYP3A4, were involved in prilocaine- and lidocaine-induced methemoglobinemia. Furthermore, the catalytic efficiencies of prilocaine and lidocaine metabolism may be involved in the different incidences of methemoglobinemia that were observed for prilocaine and lidocaine. The results obtained in this study will provide valuable information regarding the importance of CES and P450 enzymes in drug toxicity.

Authorship Contributions

Participated in research design: Higuchi, Fukami, Nakajima, Yokoi.
Conducted experiment: Higuchi, Fukami.
Contributed new reagent or analytic tools: Higuchi, Fukami.
Performed data analysis: Higuchi.
Wrote or contributed to the writing of the manuscript: Higuchi, Fukami, Yokoi.

References

Chauret N, Gauthier A, and Nicoll-Griffith DA (1998) Effect of common organic solvents on in vitro cytochrome P450-mediated metabolic activities in human liver microsomes. Drug Metab Dispos 26:1-4.

Climie CR, McLean S, Starmer GA, and Thomas J (1967) Methaemoglobinaemia in mother and foetus following continuous epidural analgesia with prilocaine. Clinical and experimental data. *Br J Anaesth* **39**:155–160.

Fukami T, Katoh M, Yamazaki H, Yokoi T, and Nakajima M (2008) Human cytochrome P450 2A13 efficiently metabolizes chemicals in air pollutants: naphthalene, styrene, and toluene. *Chem Res Toxicol* **21**:720–725.

Fukami T, Nakajima M, Sakai H, Katoh M, and Yokoi T (2007) CYP2A13 metabolizes the substrates of human CYP1A2, phenacetin, and theophylline. *Drug Metab Dispos* **35**:335–339.

Fukami T, Takahashi S, Nakagawa N, Maruichi T, Nakajima M, and Yokoi T (2010) In vitro evaluation of inhibitory effects of antidiabetic and antihyperlipidemic drugs on human carboxylesterase activities. *Drug Metab Dispos* **38**:2173–2178.

Fukami T and Yokoi T (2012) The emerging role of human esterases. *Drug Metab Pharmacokinet* **27**:466–477.

Fuller RW (1978) Structure-activity relationships among the halogenated amphetamines. *Ann N Y Acad Sci* **305**:147–159.

Ganesan S, Sahu R, Walker LA, and Tekwani BL (2010) Cytochrome P450-dependent toxicity of dapsone in human erythrocytes. *J Appl Toxicol* **30**:271–275.

Guay J (2009) Methemoglobinemia related to local anesthetics: a summary of 242 episodes. *Anesth Analg* **108**:837–845.

Guengerich FP (2008) Cytochrome p450 and chemical toxicology. *Chem Res Toxicol* **21**:70–83.

Hjelm M, Ragnarsson B, and Wistrand P (1972) Biochemical effects of aromatic compounds. 3. Ferrihaemoglobinaemia and the presence of *p*-hydroxy-*o*-toluidine in human blood after the administration of prilocaine. *Biochem Pharmacol* **21**:2825–2834.

Imai T, Taketani M, Shii M, Hosokawa M, and Chiba K (2006) Substrate specificity of carboxylesterase isozymes and their contribution to hydrolase activity in human liver and small intestine. *Drug Metab Dispos* **34**:1734–1741.

Keenaghan JB and Boyes RN (1972) The tissue distribution, metabolism and excretion of lidocaine in rats, guinea pigs, dogs and man. *J Pharmacol Exp Ther* **180**:454–463.

Kobayashi Y, Fukami T, Higuchi R, Nakajima M, and Yokoi T (2012) Metabolic activation by human arylacetamide deacetylase, CYP2E1, and CYP1A2 causes phenacetin-induced methemoglobinemia. *Biochem Pharmacol* **84**:1196–1206.

Kreutz RW and Kinni ME (1983) Life-threatening toxic methemoglobinemia induced by prilocaine. *Oral Surg Oral Med Oral Pathol* **56**:480–482.

Lindstrom HV, Bowie WC, Wallace WC, Nelson AA, and Fitzhugh OG (1969) The toxicity and metabolism of mesidine and pseudocumidine in rats. *J Pharmacol Exp Ther* **167**:223–234.

Lipkind GM and Fozzard HA (2005) Molecular modeling of local anesthetic drug binding by voltage-gated sodium channels. *Mol Pharmacol* **68**:1611–1622.

Maimo G and Redick E (2004) Recognizing and treating methemoglobinemia: a rare but dangerous complication of topical anesthetic or nitrate overdose. *Dimens Crit Care Nurs* **23**:116–118.

Moore TJ, Walsh CS, and Cohen MR (2004) Reported adverse event cases of methemoglobinemia associated with benzocaine products. *Arch Intern Med* **164**:1192–1196.

Nakajima A, Fukami T, Kobayashi Y, Watanabe A, Nakajima M, and Yokoi T (2011) Human arylacetamide deacetylase is responsible for deacetylation of rifamycins: rifampicin, rifabutin, and rifapentine. *Biochem Pharmacol* **82**:1747–1756.

Nakajima M, Tane K, Nakamura S, Shimada N, Yamazaki H, and Yokoi T (2002) Evaluation of approach to predict the contribution of multiple cytochrome P450s in drug metabolism using relative activity factor: effects of the differences in expression levels of NADPH-cytochrome P450 reductase and cytochrome $b_{(5)}$ in the expression system and the differences in the marker activities. *J Pharm Sci* **91**:952–963.

Neuhaeuser C, Weigand N, Schaaf H, Mann V, Christophis P, Howaldt HP, and Heckmann M (2008) Postoperative methemoglobinemia following infiltrative lidocaine administration for combined anesthesia in pediatric craniofacial surgery. *Paediatr Anaesth* **18**:125–131.

Onji Y and Tyuma I (1965) Methemoglobin formation by a local anesthetic and some related compounds. *Acta Anaesthesiol Scand Suppl* **16**:151–159.

Rawden HC, Kokwaro GO, Ward SA, and Edwards G (2000) Relative contribution of cytochromes P-450 and flavin-containing monoxygenases to the metabolism of albendazole by human liver microsomes. *Br J Clin Pharmacol* **49**:313–322.

Rehman HU (2001) Methemoglobinemia. *West J Med* **175**:193–196.

Reilly TP, Woster PM, and Svensson CK (1999) Methemoglobin formation by hydroxylamine metabolites of sulfamethoxazole and dapsone: implications for differences in adverse drug reactions. *J Pharmacol Exp Ther* **288**:951–959.

Rodriguez LF, Smolik LM, and Zbehlik AJ (1994) Benzocaine-induced methemoglobinemia: report of a severe reaction and review of the literature. *Ann Pharmacother* **28**:643–649.

Spooren AA and Evelo CT (2000) A study on the interaction between hydroxylamine analogues and oxyhemoglobin in intact erythrocytes. *Blood Cells Mol Dis* **26**:373–386.

Vasters FG, Eberhart LH, Koch T, Kranke P, Wulf H, and Morin AM (2006) Risk factors for prilocaine-induced methaemoglobinaemia following peripheral regional anaesthesia. *Eur J Anaesthesiol* **23**:760–765.

Wang JS, Backman JT, Taavitsainen P, Neuvonen PJ, and Kivistö KT (2000) Involvement of CYP1A2 and CYP3A4 in lidocaine *N*-deethylation and 3-hydroxylation in humans. *Drug Metab Dispos* **28**:959–965.

Watanabe A, Fukami T, Nakajima M, Takamiya M, Aoki Y, and Yokoi T (2009) Human arylacetamide deacetylase is a principal enzyme in flutamide hydrolysis. *Drug Metab Dispos* **37**:1513–1520.

Watanabe A, Fukami T, Takahashi S, Kobayashi Y, Nakagawa N, Nakajima M, and Yokoi T (2010) Arylacetamide deacetylase is a determinant enzyme for the difference in hydrolase activities of phenacetin and acetaminophen. *Drug Metab Dispos* **38**:1532–1537.

Address correspondence to: Dr. Tatsuki Fukami, Drug Metabolism and Toxicology, Faculty of Pharmaceutical Sciences, Kanazawa University, Kakuma-machi, Kanazawa 920-1192, Japan. E-mail: tatsuki@p.kanazawa-u.ac.jp

1521-009X/41/9/1738–1743$25.00
DRUG METABOLISM AND DISPOSITION

http://dx.doi.org/10.1124/dmd.113.051201
Drug Metab Dispos 41:1738–1743, October 2013

DMD
DRUG METABOLISM AND DISPOSITION
aspet

Special Section on Epigenetic Regulation of Drug Metabolizing Enzymes and Transporters

Epigenetic Regulation Is a Crucial Factor in the Repression of UGT1A1 Expression in the Human Kidney

Shingo Oda, Tatsuki Fukami, Tsuyoshi Yokoi, and Miki Nakajima

Drug Metabolism and Toxicology, Faculty of Pharmaceutical Sciences, Kanazawa University, Kakuma-machi, Kanazawa, Japan

Received January 24, 2013; accepted February 11, 2013

ABSTRACT

Human uridine 5′-diphospho-glucuronosyltransferase (UGT) 1A1 catalyzes the metabolism of numerous clinically and pharmacologically important compounds, such as bilirubin and SN-38. UGT1A1 is predominantly expressed in the liver and intestine but not in the kidney. The purpose of this study was to uncover the mechanism of the tissue-specific expression of UGT1A1, focusing on its epigenetic regulation. Bisulfite sequence analysis revealed that the CpG-rich region near the *UGT1A1* promoter (−85 to +40) was hypermethylated (83%) in the kidney, whereas it was hypomethylated (37%) in the liver. A chromatin immunoprecipitation assay demonstrated that histone H3 near the promoter was hypoacetylated in the kidney but hyperacetylated in the liver; this hyperacetylation was accompanied by the recruitment of hepatocyte nuclear factor (HNF) 1α to the promoter. The *UGT1A1* promoter in human kidney-derived HK-2 cells that do not express UGT1A1 was fully methylated, but this promoter was relatively unmethylated in human liver-derived HuH-7 cells that express UGT1A1. Treatment with 5-aza-2′-deoxycytidine (5-aza-dC), an inhibitor of DNA methylation, resulted in an increase of UGT1A1 mRNA expression in both cell types, but the increase was much larger in HK-2 cells than in HuH-7 cells. The transfection of an HNF1α expression plasmid into the HK-2 cells resulted in an increase of UGT1A1 mRNA only in the presence of 5-aza-dC. In summary, we found that DNA hypermethylation, along with histone hypoacetylation, interferes with the binding of HNF1α, resulting in the defective expression of UGT1A1 in the human kidney. Thus, epigenetic regulation is a crucial determinant of tissue-specific expression of UGT1A1.

Introduction

Uridine 5′-diphospho-glucuronosyltransferases (UGTs) catalyze the glucuronidation of a large number of endogenous and exogenous compounds. In humans, there are 19 functional UGT enzymes; these enzymes are classified into three subfamilies, UGT1A, UGT2A, and UGT2B (Mackenzie et al., 2005). The *UGT1A* genes, located on chromosome 2q37, contain multiple unique first exons and common exons 2 to 5, and they encode nine kinds of functional UGT1A enzymes (Ritter et al., 1992). The *UGT2* genes, located on chromosome 4q13, comprise six exons that are not shared between the UGT2 family members, with the exception of UGT2A1 and UGT2A2, which are formed by exon sharing as in UGT1A. The *UGT2* genes encode three UGT2A and seven UGT2B functional enzymes.

Human UGTs show tissue-specific expression. Although most UGTs are predominantly expressed in the liver, UGT1A7, UGT1A8, and UGT1A10 are exclusively expressed in the gastrointestinal tract (Strassburg et al., 1997, 1998). UGT1A1 is expressed in the liver, small intestine, and colon, but not in the kidney (Nakamura et al., 2008; Ohno and Nakajin, 2009; Court et al., 2012). The expression of UGT2A1 and 2A2 are limited to the olfactory epithelium (Court et al., 2012). UGT2B7 is abundantly expressed in the liver, kidney, small intestine, and colon, whereas UGT2B10 is expressed only in the liver (Court et al., 2012). To understand the underlying mechanisms of the tissue specific-expression of UGTs, some studies were conducted with a focus on transcriptional regulation (Gardner-Stephen and Mackenzie, 2008; Mackenzie et al., 2010). It has been demonstrated that the intestine-specific transcription factor, caudal-type homeobox protein 2 (Cdx2), as well as Sp1 and hepatocyte nuclear factor (HNF) 1α regulate UGT1A8 and 1A10 expression in the intestine (Gregory et al., 2004). HNF1α and Cdx2 cooperatively regulate UGT2B7 expression in the intestine, whereas HNF1α and octamer transcription factor-1 cooperatively regulate its expression in the liver and kidney (Gregory et al., 2006). HNF1α is also involved in the regulation of UGT1A1 expression in the liver (Bernard et al., 1999). Thus, knowledge of the transcriptional regulation of the tissue-specific expression of the UGTs is accumulating.

However, a question that has yet to be answered is why UGT1A1 is not expressed in the kidney, even though HNF1α is expressed in this tissue (Rey-Campos et al., 1991). In this study, we sought

dx.doi.org/10.1124/dmd.113.051201.

ABBREVIATIONS: 5-aza-dC, 5-aza-2′-deoxycytidine; ChIP, chromatin immunoprecipitation; GAPDH, glyceraldehyde-3-phosphate dehydrogenase; HNF, hepatocyte nuclear factor; PCR, polymerase chain reaction; TSA, trichostatin A; UGT, uridine 5′-diphospho-glucuronosyltransferase.

to clarify the mechanisms underlying the defective expression of UGT1A1, with a focus on epigenetic regulation. It is known that epigenetic changes, including DNA methylation and histone modification, are key regulators of tissue-dependent gene expression (Shiota, 2004; Ohgane et al., 2008). Supporting our hypothesis, a previous study found that the DNA methylation status of the proximal promoter region of the *UGT1A1* gene affects UGT1A1 expression in colon cancer cell lines (Gagnon et al., 2006). We investigated whether DNA methylation of the promoter and histone modification might be determinants of the tissue-specific expression of human UGT1A1.

Materials and Methods

Materials. 5-Aza-2′-deoxycytidine (5-Aza-dC) and trichostatin A (TSA) were purchased from Sigma-Aldrich (St. Louis, MO). Goat anti-human HNF1α polyclonal antibody (C-19), mouse anti-β-actin monoclonal antibody (C-14), and control rabbit and goat IgGs were purchased from Santa Cruz Biotechnology (Santa Cruz, CA). Rabbit anti-human acetyl histone H3 polyclonal antibody was purchased from Millipore (Billerica, MA). Primers were commercially synthesized at Hokkaido System Science (Sapporo, Japan). All other chemicals and solvents were of the highest grade commercially available.

Human Tissues. Human liver and kidney samples from five Japanese donors (donor 1, an 80-year-old woman; donor 2, a 54-year-old man; donor 3, a 39-year-old woman; donor 4, a 13-year-old boy; donor 5, a 40-year-old man) were obtained from autopsy materials that were discarded after pathologic investigation. The use of the human livers and kidneys was approved by the ethics committees of Kanazawa University (Kanazawa, Japan) and Iwate Medical University (Morioka, Japan).

Cell Culture. Human kidney tubular epithelial cell line HK-2 and human hepatocellular carcinoma cell line HuH-7 were obtained from the American Type Culture Collection (Manassas, VA) and the RIKEN BioResource Center (Ibaraki, Japan), respectively. These cells were cultured as previously described (Nakamura et al., 2008).

RNA Isolation and Real-Time Polymerase Chain Reaction. Total RNA was isolated from human liver and kidney samples using RNAiso (Takara Bio, Otsu, Japan) according to the manufacturer's protocol. The cDNA was synthesized from the total RNA using ReverTra Ace (Toyobo, Osaka, Japan). The UGT1A1 mRNA levels were determined by real-time polymerase chain reaction (PCR) and normalized with glyceraldehyde-3-phosphate dehydrogenase (GAPDH) mRNA levels as described previously (Izukawa et al., 2009).

Genomic DNA Extraction and Bisulfite Reaction. Genomic DNA samples were prepared from human liver (donor 3) and kidney (donor 1) samples, cell lines, or human hepatocytes (HH268, a 54-year-old Caucasian woman; Tissue Transformation Technologies, Edison, NJ) with a Gentra Puregene Tissue kit (Qiagen, Valencia, CA). Five hundred nanograms of genomic DNA digested with *EcoR* I were treated with bisulfite using the EZ DNA Methylation kit (Zymo Research, Orange, CA). The DNA fragment near the transcription start site of the *UGT1A1* gene was amplified by PCR using the primer pair shown in Table 1. The PCR products were cloned into the pT7Blue T-Vector (Novagen, Madison, WI), and randomly picked clones were sequenced. The DNA methylation status of the sequence was analyzed using the web-based tool QUMA (Kumaki et al., 2008).

Chromatin Immunoprecipitation Assay. The chromatin immunoprecipitation (ChIP) assay was performed using the ChIP assay kit (Millipore) with slight modifications. Approximately 200 mg of frozen human liver (donor 3) or kidney (donor 1) was minced on ice and suspended in 1% (v/v) formaldehyde to cross-link proteins to DNA. After centrifugation, the precipitate was resuspended in cell lysis buffer and homogenized using a Dounce homogenizer. After centrifugation, the precipitate was resuspended in nuclei lysis buffer and sonicated to shear the genomic DNA. After centrifugation, the supernatant (100 μl) was diluted 10-fold with immunoprecipitation dilution buffer and incubated with Dynabeads protein G (Life Technologies, Gaithersburg, MD) conjugated to antibodies against acetylated histone H3 (5 μg) or HNF1α (2 μg). A proportion of the diluted supernatant was kept as an input. The Dynabeads protein G was precipitated and washed sequentially one time each with a low-salt immune complex wash buffer, a high-salt immune complex buffer, and a lithium chloride immune complex buffer. The DNA-protein complex was eluted with elution buffer twice, and the cross-links were reversed by adding sodium chloride. DNA was extracted by phenol-chloroform extraction and ethanol precipitation. The −118 to + 91 region of the *UGT1A1* gene was amplified by real-time PCR with the primers shown in Table 1. The protocol for the PCR was as follows: 95°C for 30 seconds, followed by 45 cycles of 94°C for 4 seconds and 62°C for 20 seconds. DNA extraction and real-time PCR were also performed for the input samples, and the data were used as a control to evaluate the enrichment of DNA in the immunoprecipitates.

Construction of an HNF1α Expression Plasmid. Human HNF1α cDNA was amplified by PCR using the primer pair shown in Table 1 and human liver cDNA as a template. The PCR product was subcloned into the pTARGET vector (Promega, Madison, MI). The nucleotide sequence was confirmed by DNA sequencing analysis.

Chemical Treatment and Transfection of Expression Plasmid into the Cells. HK-2 and HuH-7 cells were seeded onto a 12-well plate at 0.5×10^5 cells/well and incubated for 24 hours. For dose response experiments, the cells were treated with 0.01, 0.1, 1, or 10 μM 5-aza-dC for 120 hours or treated with 50, 100, or 300 nM TSA for 24 hours and then subjected to RNA isolation. For the overexpression of HNF1α, the cells were transiently transfected with 0.5 μg of an HNF1α expression plasmid or an empty pTARGET plasmid using the X-tremeGENE HP DNA transfection reagent (Roche Applied Science, Indianapolis, IN). After 12 hours, the cells were treated with 0.1 μM 5-aza-dC for 96 hours, followed by treatment with TSA for an additional 24 hours. The UGT1A1 mRNA levels were determined as previously described.

Preparation of Nuclear Extract and Immunoblot Analysis of HNF1α. Nuclear extract was prepared from HK-2 and HuH-7 cells transfected with the HNF1α expression plasmid or empty plasmid using NE-PER Nuclear and Cytoplasmic Extraction Reagents (Thermo Fisher Scientific, Rockford, IL) according to the manufacturer's protocols. The protein concentration

TABLE 1

Oligonucleotides used for the UGT1A1 bisulfite analysis and ChIP assay and for the cloning of HNF1α

Nucleotides are numbered with the transcription start site designated as +1 in the *UGT1A1* genomic DNA sequence and base A in the initiation codon ATG designated as +1 in the HNF1α cDNA sequence.

Oligonucleotides	5′ to 3′ Sequence	Position
Bisulfite analysis of UGT1A1		
Forward	TTTGTGGATTGATAGTTTTTTATAG	−113 to −89
Reverse	CAATAACTACCATCCACTAAAATC	+134 to +111
ChIP assay of UGT1A1		
Forward	CTACCTTTGTGGACTGACAGC	−118 to −98
Reverse	CAACAGTATCTTCCCAGCATG	+111 to +91
Cloning of HNF1α		
Forward	GCAGCCGAGCCATGGTTTCT	−11 to +9
Reverse	GGTGCCGTGGTTACTGGGA	+1906 to +1888

ChIP, chromatin immunoprecipitation; HNF, hepatocyte nuclear factor; UGT, uridine 5′-diphospho-glucuronosyltransferase.

was determined using Bradford protein assay reagent (Bio-Rad Laboratories, Hercules, CA) with γ-globulin as a standard. The nuclear extract (40 μg) was separated by 7.5% SDS-PAGE and transferred to an Immobilon-P transfer membrane (Millipore). The membranes were probed with goat anti-human HNF1α or rabbit anti-human GAPDH antibodies followed by fluorescent dye-conjugated second antibodies. The membranes were then scanned using the Odyssey Infrared Imaging system (LI-COR Biosciences, Lincoln, NE).

Statistical Analyses. For DNA methylation status, the statistical significance was evaluated by the Mann-Whitney *U*-test or Fisher's exact test using the web-based tool QUMA. For mRNA expression, statistical significance was determined using an unpaired, two-tailed Student's *t* test or one-way analysis of variance followed by Dunnett's test. When the *P* value was less than 0.05, the differences were considered to be statistically significant.

Results

UGT1A1 mRNA Expression in Human Liver and Kidney. UGT1A1 mRNA expression in human liver and kidney was determined by real-time PCR. As shown in Fig. 1, UGT1A1 mRNA was detected in the liver but was negligible in the kidney. The results supported previous studies (Nakamura et al., 2008; Ohno and Nakajin, 2009) that reported the repressed expression of UGT1A1 in the human kidney.

DNA Methylation Status of the *UGT1A1* Promoter Region in Human Liver and Kidney. Genomic DNA extracted from the liver and kidney was treated with bisulfite, and the promoter region of UGT1A1 spanning −113 to +111 was amplified by PCR. The PCR product was subcloned into a vector, and 14 clones from each sample were sequenced. The DNA methylation status of the CpG dinucleotides at −85, −54, −12, +12, +36, and +40 of the *UGT1A1* gene is shown in Fig. 2. In the liver, 31 out of 84 CpG sites (37%) were methylated, whereas in the kidney, 70 out of 84 CpGs (83%) were methylated ($P = 0.07$, Mann-Whitney *U* test). Notably, the methylated CpG sites were biased in five clones in the liver. We surmised that these clones might be from hepatic nonparenchymal cells. Hence, we investigated the DNA methylation status of the *UGT1A1* promoter in human hepatocytes and found that the methylated status was only 24% (20 out of 84 CpG sites). In particular, nucleotide positions −85, −54, and −12 were unmethylated in all hepatocyte clones but were hypermethylated in the kidney ($P < 0.001$; $P < 0.01$; and $P < 0.0001$, respectively; Fisher's exact test). Thus, the DNA methylation status of the UGT1A1 promoter region is different in the liver and kidney.

Histone H3 Acetylation Status and Recruitment of HNF1α to the *UGT1A1* Promoter Region. DNA methylation induces chromatin condensation by recruiting chromatin-remodeling factors, such as methyl-CpG-binding protein and histone deacetylase, thus limiting the access of transcription factors (Bird and Wolffe, 1999). We performed ChIP assays to determine the extent of histone H3 acetylation at the *UGT1A1* promoter in the liver and kidney. In addition, the extent of the recruitment of HNF1α to the *UGT1A1* promoter in the liver and kidney was also determined because it has been demonstrated that HNF1α regulates UGT1A1 expression (Bernard et al., 1999). As

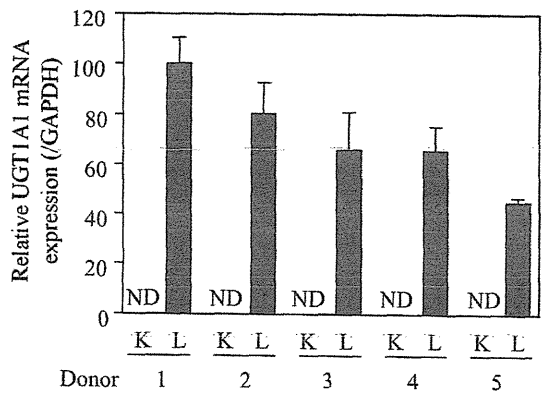

Fig. 1. UGT1A1 mRNA expression in human kidney and liver. The expression levels of UGT1A1 mRNA were determined by real-time PCR and normalized to GAPDH mRNA levels. Each kidney and liver sample with a given number of donors came from the same donors. The values are expressed as relative to the UGT1A1 levels in the liver from donor 1. Each column represents the mean ± S.D. of triplicate determinations. K, kidney; L, liver; ND, not detectable.

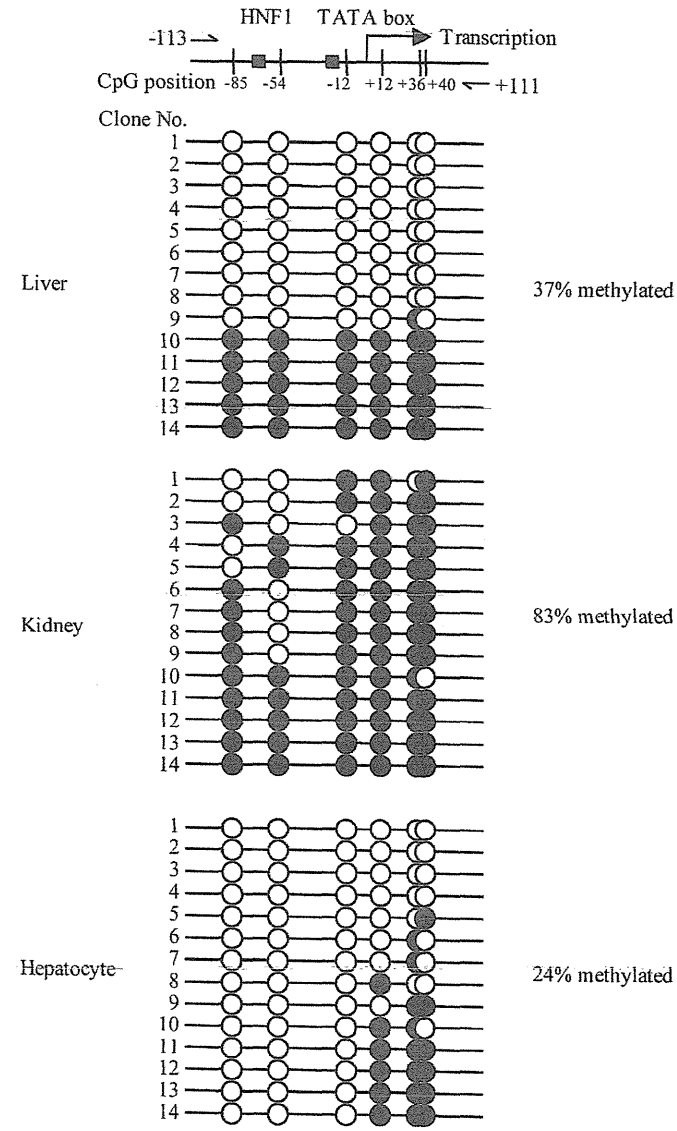

Fig. 2. DNA methylation status of the *UGT1A1* promoter region in human liver, kidney or hepatocytes. Top panel shows a schematic diagram of the *UGT1A1* 5′-flanking region. The vertical lines and numbers represent the position of the cytosine residues of the CpGs relative to the transcription start site as +1. The HNF1 binding site and TATA box are represented by rectangles. Arrows indicate the positions of the primers used for ChIP analysis. Bottom panel shows DNA methylation status of CpG sites. Bisulfite sequencing analysis was performed using genomic DNAs extracted from human liver (donor 3), kidney (donor 1) or hepatocytes (HH268). Fourteen clones from each sample type were sequenced. The open and closed circles represent unmethylated and methylated cytosines, respectively.

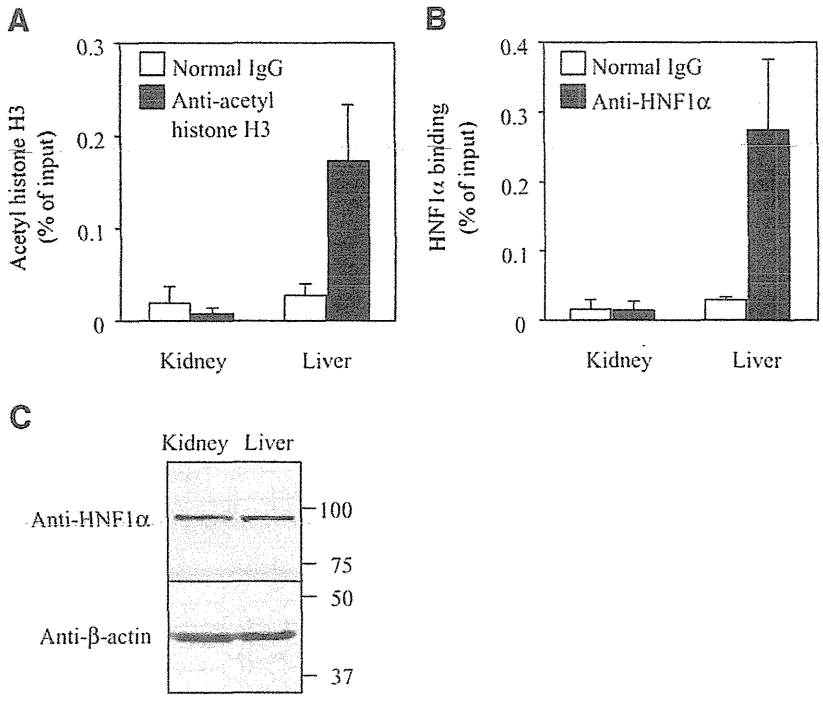

Fig. 3. Histone H3 acetylation and recruitment of HNF1α in the *UGT1A1* promoter region in human kidney and liver. (A and B) ChIP assay of acetyl histone H3 and HNF1α in kidney and liver. Human kidney (donor 1) and liver (donor 3) chromatin was precipitated with anti-acetyl histone H3 antibody (A) or anti-HNF1α antibody (B). The precipitated DNA was quantified by real-time PCR with a primer pair that amplified the region from −118 to +111 of the *UGT1A1* gene. The results are expressed as the percentage of input. Normal rabbit or goat IgGs (open columns) were included as negative controls. (C) Western blot analysis of HNF1α in kidney and liver. Homogenates (50 μg) from kidney and liver samples were subjected to 10% SDS-PAGE and probed with anti-HNF1α or anti-β-actin antibodies. Each column represents the mean ± S.D. of triplicate determinations.

shown in Fig. 3A, acetylated histone H3 was enriched at the *UGT1A1* promoter in the liver but not in the kidney. In addition, it was demonstrated that HNF1α was highly recruited to the *UGT1A1* promoter in the liver but not in the kidney (Fig. 3B). Western blot analysis demonstrated that HNF1α is expressed in kidney and liver equally (Fig. 3C). These results suggest that the DNA hypermethylation in the kidney could be linked to abolished histone H3 acetylation and HNF1α binding.

Effects of the Inhibition of DNA Methylation and Histone Deacetylation and the Transfection of Exogenous HNF1α on UGT1A1 Expression. To investigate the significance of the DNA methylation at the promoter region in the repression of UGT1A1 expression, we performed a series of experiments using cell lines. We selected two cell lines, the human kidney-derived HK-2 line and liver-derived HuH-7 cells. We found that the *UGT1A1* promoter region was hypermethylated (98%) in HK-2 cells but was moderately methylated (47%) in HuH-7 cells ($P < 0.0001$, Fig. 4A). UGT1A1 mRNA was marginally expressed in HK-2 cells but was substantially expressed in HuH-7 cells (~4800-fold difference) (Fig. 4B), suggesting that DNA methylation negatively regulates UGT1A1 expression in HK-2 cells. To investigate whether the inhibition of DNA methylation could induce UGT1A1 expression, the cells were treated with 5-aza-dC, an inhibitor of DNA methylation. Although this treatment increased UGT1A1 mRNA in both cell lines, the induction was higher in HK-2 cells (~400-fold at maximum) than in HuH-7 cells (~6-fold at maximum) (Fig. 4B). We confirmed that 5-aza-dC treatment efficiently decreased the methylation status in HK-2 to 33% ($P < 0.001$) and in HuH-7 cells to 7% ($P < 0.001$) (Fig. 4C).

The UGT1A1 mRNA level in HK-2 cells treated with 0.1 μM 5-aza-dC was still low compared with that in HuH-7 cells. We suspected that HNF1α might be lacking in HK-2 cells, thus causing the lower UGT1A1 levels. Western blot analysis demonstrated that HNF1α is expressed at very low levels in HK-2 cells (Fig. 4D). To investigate the significance of the DNA methylation status in the suppression of UGT1A1 expression, we sought to exogenously express HNF1α in HK-2 cells. The HNF1α protein level was dramatically increased by the transfection of the HNF1α expression plasmid into HK-2 cells (Fig. 4D), but UGT1A1 mRNA expression was not increased (Fig. 4E). These results suggested that DNA methylation inhibits the binding of HNF1α to the promoter of UGT1A1. However, under 5-aza-dC treatment, the overexpression of HNF1α resulted in a significant increase of UGT1A1 mRNA expression (4.3-fold) in HK-2 cells. This phenomenon was not observed in HuH-7 cells, implying that endogenous HNF1α expression levels might be sufficient for UGT1A1 in HuH-7 cells (Fig. 4D).

Finally, we investigated whether histone deacetylation is also involved in the repression of UGT1A1 expression. When the HK-2 and HuH-7 cells were treated with TSA, an inhibitor of histone deacetylation, UGT1A1 mRNA expression was unchanged (Fig. 4E). However, TSA treatment facilitated (by 1.7-fold) the increase of UGT1A1 mRNA by 5-aza-dC treatment in HK-2 cells in the presence of exogenously expressed HNF1α. This result was not observed in HuH-7 cells. Collectively, these results suggest that DNA methylation status, and to a lesser extent histone deacetylation status, are critical determinants of UGT1A1 expression.

Discussion

Human UGT1A1 is predominantly expressed in the liver and the intestine but not in the kidney. Previous studies demonstrated that HNF1α and HNF1β are involved in the constitutive (Bernard et al., 1999) and inducible expression of UGT1A1 (Sugatani et al., 2008) by binding to a site approximately 30 bp upstream of the TATA box. The expression of HNF1α and HNF1β is not confined to the liver, as these genes are expressed in various tissues, including the kidney, intestine, stomach, and pancreas (Harries et al., 2006). Therefore, the reason for the repressed expression of UGT1A1 in the kidney remained to be clarified. To uncover the underlying mechanism, we conducted studies focusing on epigenetic regulation. HNF1α and HNF1β form homodimers or heterodimers and equally *trans*-activate the *UGT1A1* gene (Bernard et al., 1999). Therefore, HNF1α was studied as the representative *UGT1A1* activator.

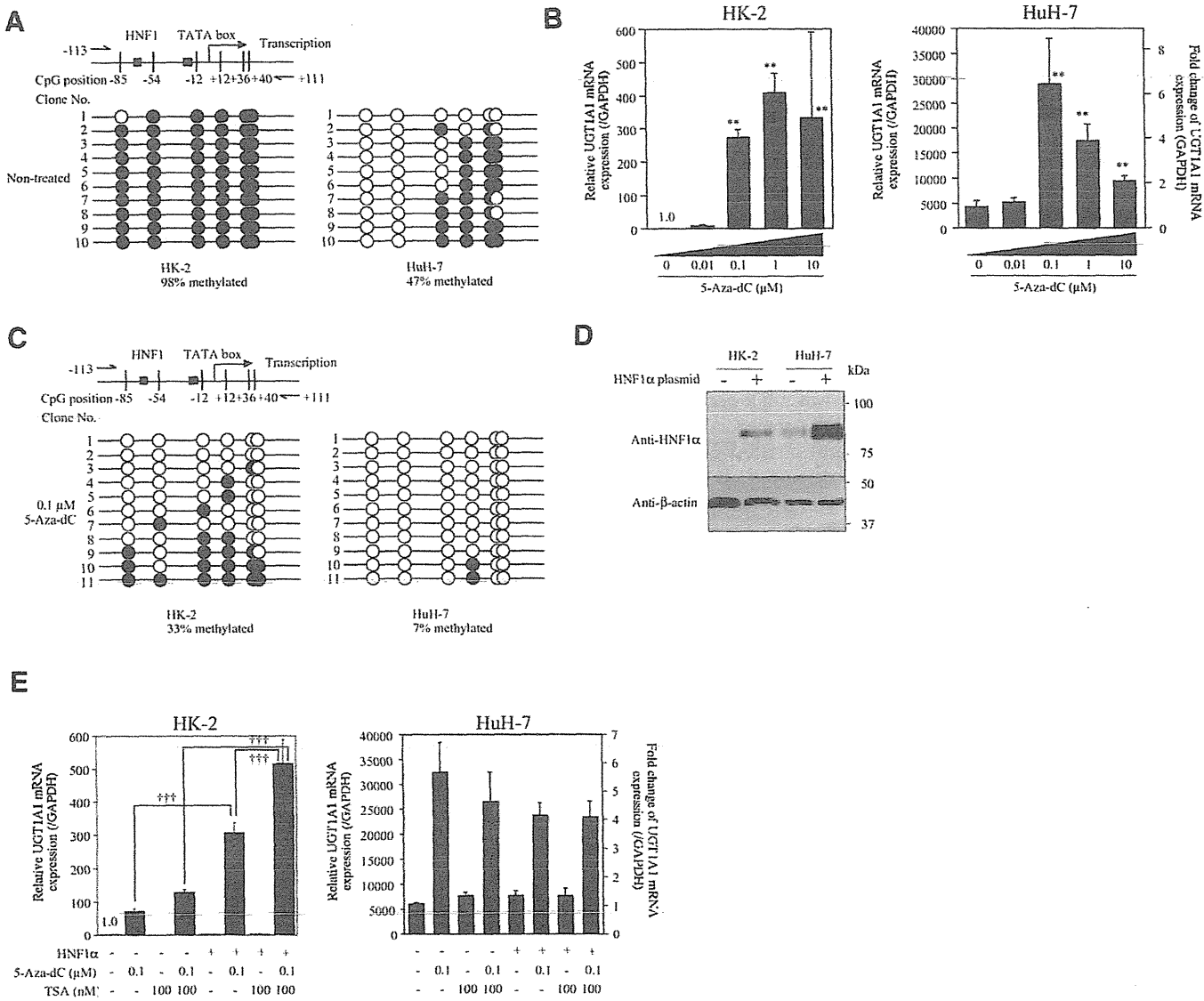

Fig. 4. Effects of 5-aza-dC and/or TSA treatment and transfection of HNF1α on the UGT1A1 expression in HK-2 and HuH-7 cells. (A) DNA methylation status of the *UGT1A1* promoter region in HK-2 and HuH-7 cells. Ten clones each were sequenced. The open and closed circles represent unmethylated and methylated cytosines, respectively. (B) Effects of 5-aza-dC on the UGT1A1 expression in HK-2 and HuH-7 cells. UGT1A1 mRNA level was determined by real-time RT-PCR and normalized with the GAPDH mRNA levels. (C) Effects of 5-aza-dC on the DNA methylation status of the *UGT1A1* promoter region in HK-2 and HuH-7 cells. Bisulfite sequencing analysis was performed using genomic DNA extracted from 5-aza-dC-treated cells. (D) Western blot analysis of HNF1α in HK-2 and HuH-7 cells. Nuclear extracts from HK-2 and HuH-7 cells transfected with HNF1α expression plasmid (+) or empty plasmid (−) were analyzed. (E) Effects of 5-aza-dC and/or TSA treatment and transfection of HNF1α on the UGT1A1 mRNA expression in HK-2 and HuH-7 cells. The cells were transiently transfected with HNF1α expression plasmid (+) or empty plasmid (−), followed by treatment with 5-aza-dC and/or TSA. The expression level of UGT1A1 mRNA was determined by real-time PCR. Data were expressed as relative to UGT1A1 expression compared with nontreated HK-2 cells. Each column represents the mean ± S.D. of triplicate determinations. $^{**}P < 0.01$, compared with nontreated cells; $^{\dagger\dagger\dagger}P < 0.001$.

We found that the CpG island at the promoter region of the *UGT1A1* gene in the kidney was hypermethylated, whereas it was hypomethylated in the liver (Fig. 2). Upon DNA methylation, gene silencing occurs by two mechanisms: 1) the methyl group physically interrupts the binding of transcription factors to their recognition sequences, and 2) methyl-CpG-binding proteins bind to the methylated DNA and recruit co-repressor molecules, including histone deacetylase, to induce chromatin structure condensation (Shiota, 2004). Previously, it was demonstrated by gel shift assay that the methylated CpG sites at the *UGT1A1* promoter did not prevent the binding of HNF1α (Bélanger et al., 2010). In contrast, the present study demonstrated that DNA hypermethylation of the *UGT1A1* promoter in the kidney was accompanied by increased acetylation of histone H3 and defective recruitment of HNF1α (Fig. 3). Therefore, gene silencing of UGT1A1 in the kidney would be due to the latter mechanism with the abolished binding of HNF1α.

Our cell line based study clearly demonstrated the significance of DNA methylation in the regulation of UGT1A1 as follows: 1) substantial expression of UGT1A1 mRNA is observed in HuH-7 cells with DNA hypomethylation status; 2) 5-aza-dC treatment resulted in an increase of UGT1A1 expression that reflected the change in methylation status; and 3) the exogenously expressed HNF1α could increase UGT1A1 expression only in the presence of 5-aza-dC in HK-2 cells. These findings clearly illustrated that unmethylated DNA is a prerequisite for the transcriptional activation of UGT1A1.

The study using TSA demonstrated that histone acetylation is a supplemental factor for transactivation, supporting the general perception (Cameron et al., 1999). In contrast to our study, a previous study reported a significant increase of UGT1A1 mRNA expression following treatment with 3 mM TSA in HepG2 cells (Mackenzie et al., 2010). When we treated the HK-2 and HuH-7 cells with 1 mM TSA, a prominent decrease of cell viability was observed. Thus, it is possible that there are inter-cell line differences in the response toward TSA. Collectively, DNA methylation at the promoter region of UGT1A1 may evoke the condensed chromatin structure through histone deacetylation, thereby inhibiting the binding of such transcription factors as HNF1α. This theory would explain the defective expression of UGT1A1 in kidney, where HNF1α is substantially expressed.

Although the simultaneous overexpression of HNF1α and inhibition of DNA methylation tremendously induced UGT1A1 mRNA in HK-2 cells, the UGT1A1 level was still lower than the level in HuH-7 cells (Fig. 4). It was surmised that some factors regulating UGT1A1 expression might be insufficient in HK-2 cells. Previous studies have reported that pregnane X receptor (Sugatani et al., 2008), glucocorticoid receptor (Usui et al., 2006), constitutive androstane receptor (Sugatani et al., 2008), peroxisome proliferator-activated receptor α (Senekeo-Effenberger et al., 2007), NF-E2-related factor-2 (Yueh and Tukey, 2007), and aryl hydrocarbon receptor (Yueh et al., 2003) are involved in UGT1A1 regulation. It is possible that such factors may be insufficient in HK-2 cells, although experimental proof is required. As another possibility, differences in histone modifications other than acetylation are feasible, namely H3K4 methylation (activating mark), H3K9 methylation (silencing mark), and H3K27 methylation (silencing mark). Thus, such factors might also be involved in the regulation of the basal expression of UGT1A1 in cell lines and tissues.

Each member of UGT1A family has a unique promoter. The tissue-specific expression of UGT1As could be attributed to the differences in their promoter activation (Gong et al., 2001). It is reasonable to assume that UGT isoforms other than UGT1A1 showing tissue-specific expression might also be epigenetically regulated. We are currently working on this issue.

In conclusion, we found that the DNA methylation status of the human *UGT1A1* promoter is different in the liver and kidney. DNA methylation, hypoacetylation of histone H3, and diminished binding of HNF1α could explain the defective expression of UGT1A1 in the kidney. A remaining future challenge is the elucidation of the degree to which UGT1A1 expression is influenced by factors affecting epigenetic status, such as aging, sex, disease, and lifestyle habits.

Acknowledgments

The authors thank Drs. Yasuhiro Aoki and Masataka Takamiya in Iwate Medical University for supplying human tissues.

Authorship Contributions

Participated in research design: Oda, Nakajima, Fukami, Yokoi.

Conducted experiments: Oda.

Performed data analysis: Oda.

Wrote or contributed to the writing of the manuscript: Oda, Nakajima, Yokoi.

References

Bélanger AS, Tojcic J, Harvey M, and Guillemette C (2010) Regulation of *UGT1A1* and *HNF1* transcription factor gene expression by DNA methylation in colon cancer cells. *BMC Mol Biol* **11**:9.

Bernard P, Goudonnet H, Artur Y, Desvergne B, and Wahli W (1999) Activation of the mouse TATA-less and human TATA-containing UDP-glucuronosyltransferase *1A1* promoters by hepatocyte nuclear factor 1. *Mol Pharmacol* **56**:526–536.

Bird AP and Wolffe AP (1999) Methylation-induced repression—belts, braces, and chromatin. *Cell* **99**:451–454.

Cameron EE, Bachman KE, Myöhänen S, Herman JG, and Baylin SB (1999) Synergy of demethylation and histone deacetylase inhibition in the re-expression of genes silenced in cancer. *Nat Genet* **21**:103–107.

Court MH, Zhang X, Ding X, Yee KK, Hesse LM, and Finel M (2012) Quantitative distribution of mRNAs encoding the 19 human UDP-glucuronosyltransferase enzymes in 26 adult and 3 fetal tissues. *Xenobiotica* **42**:266–277.

Gagnon JF, Bernard O, Villeneuve L, Têtu B, and Guillemette C (2006) Irinotecan inactivation is modulated by epigenetic silencing of *UGT1A1* in colon cancer. *Clin Cancer Res* **12**: 1850–1858.

Gardner-Stephen DA and Mackenzie PI (2008) Liver-enriched transcription factors and their role in regulating UDP glucuronosyltransferase gene expression. *Curr Drug Metab* **9**:439–452.

Gong QH, Cho JW, Huang T, Potter C, Gholami N, Basu NK, Kubota S, Carvalho S, Pennington MW, and Owens IS, et al. (2001) Thirteen UDPglucuronosyltransferase genes are encoded at the human UGT1 gene complex locus. *Pharmacogenetics* **11**:357–368.

Gregory PA, Gardner-Stephen DA, Rogers A, Michael MZ, and Mackenzie PI (2006) The caudal-related homeodomain protein Cdx2 and hepatocyte nuclear factor 1α cooperatively regulate the UDP-glucuronosyltransferase 2B7 gene promoter. *Pharmacogenet Genomics* **16**:527–536.

Gregory PA, Lewinsky RH, Gardner-Stephen DA, and Mackenzie PI (2004) Coordinate regulation of the human UDP-glucuronosyltransferase *1A8, 1A9*, and *1A10* genes by hepatocyte nuclear factor 1α and the caudal-related homeodomain protein 2. *Mol Pharmacol* **65**:953–963.

Harries LW, Ellard S, Stride A, Morgan NG, and Hattersley AT (2006) Isomers of the *TCF1* gene encoding hepatocyte nuclear factor-1 alpha show differential expression in the pancreas and define the relationship between mutation position and clinical phenotype in monogenic diabetes. *Hum Mol Genet* **15**:2216–2224.

Izukawa T, Nakajima M, Fujiwara R, Yamanaka H, Fukami T, Takamiya M, Aoki Y, Ikushiro S, Sakaki T, and Yokoi T (2009) Quantitative analysis of UDP-glucuronosyltransferase (UGT) 1A and UGT2B expression levels in human livers. *Drug Metab Dispos* **37**:1759–1768.

Kumaki Y, Oda M, and Okano M (2008) QUMA: quantification tool for methylation analysis. *Nucleic Acids Res* **36** (Web Server issue):W170-5.

Mackenzie PI, Bock KW, Burchell B, Guillemette C, Ikushiro S, Iyanagi T, Miners JO, Owens IS, and Nebert DW (2005) Nomenclature update for the mammalian UDP glycosyltransferase (*UGT*) gene superfamily. *Pharmacogenet Genomics* **15**:677–685.

Mackenzie PI, Hu DG, and Gardner-Stephen DA (2010) The regulation of UDP-glucuronosyltransferase genes by tissue-specific and ligand-activated transcription factors. *Drug Metab Rev* **42**:99–109.

Nakamura A, Nakajima M, Yamanaka H, Fujiwara R, and Yokoi T (2008) Expression of UGT1A and UGT2B mRNA in human normal tissues and various cell lines. *Drug Metab Dispos* **36**: 1461–1464.

Ohgane J, Yagi S, and Shiota K (2008) Epigenetics: the DNA methylation profile of tissue-dependent and differentially methylated regions in cells. *Placenta* **29 (Suppl A)**:S29-S35.

Ohno S and Nakajin S (2009) Determination of mRNA expression of human UDP-glucuronosyltransferases and application for localization in various human tissues by real-time reverse transcriptase-polymerase chain reaction. *Drug Metab Dispos* **37**:32–40.

Rey-Campos J, Chouard T, Yaniv M, and Cereghini S (1991) vHNF1 is a homeoprotein that activates transcription and forms heterodimers with HNF1. *EMBO J* **10**:1445–1457.

Ritter JK, Yeatman MT, Ferreira P, and Owens IS (1992) Identification of a genetic alteration in the code for bilirubin UDP-glucuronosyltransferase in the *UGT1* gene complex of a Crigler-Najjar type I patient. *J Clin Invest* **90**:150–155.

Senekeo-Effenberger K, Chen S, Brace-Sinnokrak E, Bonzo JA, Yueh MF, Argikar U, Kaeding J, Trottier J, Remmel RP, and Ritter JK, et al. (2007) Expression of the human UGT1 locus in transgenic mice by 4-chloro-6-(2,3-xylidino)-2-pyrimidinylthioacetic acid (WY-14643) and implications on drug metabolism through peroxisome proliferator-activated receptor α activation. *Drug Metab Dispos* **35**:419–427.

Shiota K (2004) DNA methylation profiles of CpG islands for cellular differentiation and development in mammals. *Cytogenet Genome Res* **105**:325–334.

Strassburg CP, Manns MP, and Tukey RH (1998) Expression of the UDP-glucuronosyltransferase 1A locus in human colon. Identification and characterization of the novel extrahepatic UGT1A8. *J Biol Chem* **273**:8719–8726.

Strassburg CP, Oldhafer K, Manns MP, and Tukey RH (1997) Differential expression of the *UGT1A* locus in human liver, biliary, and gastric tissue: identification of *UGT1A7* and *UGT1A10* transcripts in extrahepatic tissue. *Mol Pharmacol* **52**:212–220.

Sugatani J, Mizushima K, Osabe M, Yamakawa K, Kakizaki S, Takagi H, Mori M, Ikari A, and Miwa M (2008) Transcriptional regulation of human *UGT1A1* gene expression through distal and proximal promoter motifs: implication of defects in the *UGT1A1* gene promoter. *Naunyn Schmiedebergs Arch Pharmacol* **377**:597–605.

Usui T, Kuno T, and Mizutani T (2006) Induction of human UDP-glucuronosyltransferase 1A1 by cortisol-GR. *Mol Biol Rep* **33**:91–96.

Yueh MF, Huang YH, Hiller A, Chen S, Nguyen N, and Tukey RH (2003) Involvement of the xenobiotic response element (XRE) in Ah receptor-mediated induction of human UDP-glucuronosyltransferase *1A1*. *J Biol Chem* **278**:15001–15006.

Yueh MF and Tukey RH (2007) Nrf2-Keap1 signaling pathway regulates human UGT1A1 expression *in vitro* and in transgenic *UGT1* mice. *J Biol Chem* **282**:8749–8758.

Address correspondence to: Dr. Miki Nakajima, Drug Metabolism and Toxicology, Faculty of Pharmaceutical Sciences, Kanazawa University, Kakuma-machi, Kanazawa 920-1192, Japan. E-mail: nmiki@p.kanazawa-u.ac.jp

Toxicology Letters 214 (2012) 9–18

Contents lists available at SciVerse ScienceDirect

Toxicology Letters

journal homepage: www.elsevier.com/locate/toxlet

Chimeric mice with a humanized liver as an animal model of troglitazone-induced liver injury

Masakazu Kakuni[a], Mayu Morita[b], Kentaro Matsuo[b], Yumiko Katoh[a], Miki Nakajima[b], Chise Tateno[a], Tsuyoshi Yokoi[b,*]

[a] PhoenixBio Co., Ltd., Hiroshima 739-0046, Japan
[b] Division of Pharmaceutical Sciences, Faculty of Pharmaceutical Sciences, Kanazawa University, Kakuma-machi, Kanazawa 920-1192, Japan

HIGHLIGHTS

- Troglitazone (Tro) was withdrawn due to its association with severe liver injury.
- Orally administered Tro has never induced liver injury in experimental animals.
- The chimeric mice with a humanized liver reproduced Tro-induced liver injury.
- Possible factors that contribute to the Tro-induced liver injury were evaluated.
- This mouse model enables human hepatocytes to be examined in an *in vivo* environment.

ARTICLE INFO

Article history:
Received 11 April 2012
Received in revised form 31 July 2012
Accepted 2 August 2012
Available online 10 August 2012

Keywords:
Chimeric mouse with a humanized liver
Drug-induced liver injury (DILI)
Hepatotoxicity
Troglitazone
Glutathione

ABSTRACT

Troglitazone (Tro) is a thiazolidinedione antidiabetic drug that was withdrawn from the market due to its association with idiosyncratic severe liver injury. Tro has never induced liver injury in experimental animals *in vivo*. It was assumed that the species differences between human and experimental animals in the pharmaco- or toxicokinetics of Tro might be associated with these observations. In this study, we investigated whether a chimeric mouse with a humanized liver that we previously established, whose replacement index with human hepatocytes is up to 92% can reproduce Tro-induced liver injury. When the chimeric mice were orally administered Tro for 14 or 23 days (1000 mg/kg/day), serum alanine aminotransferase (ALT) was significantly increased by 2.1- and 3.6-fold, respectively. Co-administration of L-buthionine sulfoximine (10 mM in drinking water), an inhibitor of glutathione (GSH) synthesis, unexpectedly prevented the Tro-dependent increase of ALT, which suggests that the GSH scavenging pathway will not be involved in Tro-induced liver injury. To elucidate the mechanism of the onset of liver injury, hepatic GSH content, the level of oxidative stress markers and phase I and phase II drug metabolizing enzymes were determined. However, these factors were not associated with Tro-induced liver injury. An immune-mediated reaction may be associated with Tro-induced liver toxicity *in vivo*, because the chimeric mouse is derived from an immunodeficient SCID mouse. In conclusion, we successfully reproduced Tro-induced liver injury using chimeric mice with a humanized liver, which provides a new animal model for studying idiosyncratic drug-induced liver injury.

1. Introduction

Troglitazone (Tro) was the first thiazolidinedione used for treating of type II diabetes mellitus, but was withdrawn due to serious idiosyncratic liver injury. During the preclinical development of Tro, no study could predict the hepatotoxic effect of Tro in human (Watanabe et al., 1999). After the withdrawal of Tro from the market, numerous studies using animal models were performed to reproduce the hepatotoxicity of Tro, but almost all were unsuccessful (Bedoucha et al., 2001; Jia et al., 2000; Watanabe et al., 2000).

Ong et al. (2007) reported that the administration of Tro (30 mg/kg, *i.p.*) to heterozygous superoxide dismutase 2 (SOD2) knockout ($SOD2^{+/-}$) mice resulted in hepatocellular necrosis and increased serum alanine aminotransferase (ALT) levels, suggesting that SOD2, which is expressed mainly in the mitochondria, plays a crucial role in Tro-induced liver injury. However, other research group could not reproduce these results using the same

* Corresponding author at: Drug Metabolism and Toxicology, Faculty of Pharmaceutical Sciences, Kanazawa University, Kakuma-machi, Kanazawa 920-1192, Japan. Tel.: +81 76 234 4407; fax: +81 76 234 4407.
E-mail address: tyokoi@kenroku.kanazawa-u.ac.jp (T. Yokoi).

0378-4274/$ – see front matter © 2012 Elsevier Ireland Ltd. All rights reserved.
http://dx.doi.org/10.1016/j.toxlet.2012.08.001

heterozygous SOD2 knockout mice (Fujimoto et al., 2009). No further studies of *in vivo* animal models have been reported.

Because idiosyncratic liver injury is a human-specific toxic event, we surmised that previously established chimeric mice with a humanized liver (Tateno et al., 2004) might be useful as an animal model. In this study, we investigated whether Tro causes liver injury in a chimeric mouse with a humanized liver, which was derived from a urokinase-type plasminogen activator$^{+/+}$/severe combined immunodeficient transgenic (uPA$^{+/+}$/SCID mouse) mouse line. In this animal model, more than 75% of the mouse hepatocytes are replaced with human hepatocytes in which the human mRNAs and proteins expression levels and enzyme activities were evaluated (Katoh et al., 2004, 2005, 2007; Nishimura et al., 2005).

Tro undergoes metabolic activation by CYPs, in particular, the CYP3A4 isoform, to form reactive metabolites that bind covalently to proteins and nucleophiles, such as glutathione (GSH) and cysteine. Various reactive metabolites of Tro were identified as GSH conjugates (Tettey et al., 2001; Kassahun et al., 2001; He et al., 2004). The susceptibility of drugs metabolized to reactive intermediates is different between GSH-depleted animals and normal animals (T. Watanabe et al., 2003; Usui et al., 2011). Therefore, we expected that Tro would exhibit hepatotoxic effects under a GSH-depleted condition. L-Buthionine sulfoximine (BSO), a well-known inhibitor of GSH synthesis, was selected to investigate the relationship between the GSH conjugation ability and Tro-induced hepatotoxicity.

In the present study, we orally administered Tro for 14 or 23 days to chimeric mice with a humanized liver and reproduced liver injury. Subsequently, possible factors that were expected to contribute to the development of Tro-induced liver injury, such as drug-metabolizing enzymes, GSH, SOD2, and protein carbonyl contents, were evaluated.

2. Materials and methods

2.1. Chemicals

TRO was kindly provided by Daiichi Sankyo (Tokyo, Japan). L-Buthionine sulfoximine (BSO) and paclitaxel were purchased from Sigma (St. Louis, MO). ReverTra Ace was from Toyobo (Tokyo, Japan). Random hexamer, RNAiso, SYBR Premix Ex Taq, and ROX Reference Dye II were from Takara (Osaka, Japan). Recombinant human CYP2C8 and CYP3A4 expressed in baculovirus-infected insect cells and 6a-hydroxypaclitaxel were from BD Gentest (Woburn, MA). Dexamethasone and testosterone were from Wako Pure Chemical Industries (Osaka, Japan). 6b-Hydroxytestosterone was from Sekisui Medical (Tokyo, Japan). All primers were commercially synthesized at Hokkaido System Sciences (Sapporo, Japan). The polyclonal rabbit anti-human CYP2C8 antibody was from Nosan (Yokohama, Japan) and the polyclonal goat anti-CYP3A antibody (sc-30621) was from Santa Cruz Biotechnology (Santa Cruz, CA). All other chemicals were of analytical or the highest grade commercially available.

2.2. Generation of the chimeric mice with a humanized liver

The present study was conducted in accordance with the National Institutes of Health Guide for Animal Welfare of Japan, and the protocols were approved by the Institutional Animal Care and Use Committees of Kanazawa University (Kanazawa, Japan) and PhoenixBio Co., Ltd. (Hiroshima, Japan). The chimeric mice were generated by PhoenixBio. Briefly, commercially available cryopreserved human hepatocytes (5-year-old African-American male from BD Gentest) were transplanted into the spleens of uPA$^{+/+}$/SCID mice at approximately 3–4 weeks of age. At mice's age of 6–7 weeks, the monitoring of human albumin (h-Alb) concentration in blood was started and continued until the start of the study when the chimeric mice were 11–15 weeks old. Two microliters of blood was collected from tail vein of the mice once per week, and the concentrations of hAlb in the blood of the chimeric mice were determined by latex agglutination immunonephelometry to estimate the rate of replacement of mouse hepatocytes with human hepatocytes (RI: Replacement Index). The correlation between hAlb and the actual RI has been determined based on immunohistochemistry conducted with anti-human specific cytokeratin 8 and 18 antibodies (Tateno et al., 2004). The chimeric mice used in the present study were female, 11–15 weeks old, and exhibited concentrations of 8.0–14.9 mg/ml of hAlb or an RI of 75–92% at the start of the TRO administration (Table 1). The animals were housed in a controlled environment (temperature 23 ± 1 °C, humidity 57 ± 15%, and 12 h light/12 h dark cycle) in the institution's animal facility with *ad libitum* access to food and water.

2.3. Drug and/or BSO administration

The chimeric mice were orally administered Tro [250 mg/kg/10 ml, 500 mg/kg/ml or 1000 mg/kg/10 ml, suspended in 0.5% carboxymethylcellulose (CMC)] once daily for 14 (1000 mg/kg), 23 (1000 mg/kg) or 28 (250 and 500 mg/kg) days in a non-fasting condition, and 0.5% CMC was administered once daily as a control. BSO (10 mM) in sterilized tap water was also administered *via* drinking water alone or with Tro. Water bottle was changed twice a week during the BSO treatment. The dosing method was originally reported by T. Watanabe et al. (2003), in which 5–30 mM of BSO in drinking water had been confirmed to be stable for 15 days at 23 °C without light-shielded conditions. Pre-dosing blood samples were collected under isoflurane anesthesia to measure the initial serum ALT level. Twenty-four hours after the last Tro administration, the blood and livers were collected by exsanguination under isoflurane anesthesia. Serum ALT, aspartate aminotransferase (AST), bilirubin (total bilirubin: T-Bil, and direct bilirubin: D-Bil) and lactate dehydrogenase (LDH) levels were measured using FUJI DRI-CHEM (FUJIFILM, Tokyo, Japan). A portion of the liver was fixed in buffered neutral 10% formalin. The fixed samples were embedded in paraffin, sectioned at a thickness of 2 μm and stained with hematoxylin–eosin (H&E) for microscopic examination.

2.4. GSH level

Mouse livers were homogenized in ice-cold 5% sulfosalicylic acid using a glass homogenizer and centrifuged at 8000 × *g* at 4 °C for 10 min. The GSH concentration in the supernatant was measured as described previously (Tietze, 1969).

2.5. Glutathione S-transferase (GST) activity

GST activity was measured according to the method of Habig et al. (1974) with slight modifications. The incubation mixtures consisted of cytosol (0.1 ml) in 125 mM potassium phosphate buffer (pH 6.5) containing 1.25 mM GSH (0.8 ml) and 10 mM 1-chloro-2,4-dinitrobenzene in 40% ethanol (0.1 ml). The reaction mixture was incubated at 25 °C for 10 min and monitored at 340 nm.

2.6. SOD2 activity

SOD2 activity was measured using a Superoxide Dismutase Assay kit (Cayman Chemical, Ann Arbor, MI). The method utilizes tetrazolium salt to quantify the superoxide radicals generated by xanthine oxidase and hypoxanthine. The standard curve was generated using a quality controlled SOD standard in the kit. SOD2 activity was determined in the presence of potassium cyanide to inhibit SOD1 activity.

2.7. Protein carbonyl content

Plasma protein carbonyl content was measured using an OxiSelect Protein Carbonyl ELISA kit (Cell Biolabs, Tokyo, Japan) as described previously (Yoshikawa et al., 2009).

2.8. Real-time reverse transcription (RT)-PCR

Total hepatic RNA was isolated using RNAiso according to the manufacturer's instructions. Human CYP2C8, CYP3A4, SULT1A1, UGT1A1 and GAPDH mRNA levels were quantified by real-time RT-PCR. Total RNA (4 μg) and 150 ng random hexamer were mixed and incubated at 70 °C for 10 min. An RNA solution was added to a reaction mixture that contained 100 units of ReverTra Ace, reaction buffer and 0.5 mM dNTPs in a final volume of 40 μl. The reaction mixture was incubated at 30 °C for 10 min, 42 °C for 1 h, and then heated at 98 °C for 10 min to inactivate the enzyme. Real-time RT-PCR was performed using the Mx3000P (Stratagene, La Jolla, CA). The PCR mixture contained 1 μl of template cDNA, SYBR Premix Ex Taq solution, and 10 pmol of sense and antisense primers. The human-specific primer sequences used in this study are shown in Table 2. The amplified products were monitored directly by measuring the intensity of the SYBR Green I dye (Molecular Probes, Eugene, OR) that binds to the PCR amplified double-stranded DNA.

2.9. Immunoblot analysis

SDS-polyacrylamide gel electrophoresis and immunoblot analysis of human CYP2C8 and CYP3A were performed according to Katoh et al. (2004). The liver microsomes (2 or 20 μg) were separated on 10% polyacrylamide gel and transferred electrophoretically to a polyvinylidene difluoride membrane. Recombinant human P450s were applied as standards. Biotinylated anti-rabbit or goat IgG and a Vectastain ABC kit (Vector Laboratories, Burlingame, CA) were used for diaminobenzidine staining. It was confirmed that the human P450 antibodies in this experimental condition did not cross-react with the mouse orthologs.

Table 1
Chimeric mice used in this study.

Group	Mouse no.	Age at 1st dose (week)	hAlb concentration in the blood (mg/ml)	Approximate RI (%)
Control	1	13	9.6	80
	2	13	11.6	85
	3	13	9.1	78
	4	11	8.0	75
	5	12	9.3	79
	6	12	11.6	85
Tro 1000 mg/kg (14 days)	7	13	11.7	85
	8	13	9.6	80
	9	13	9.1	78
	10	14	9.7	80
	11	13	9.6	80
Tro 250 mg/kg (28 days)	S1	12	9.3	79
	S2	12	8.4	76
	S3	12	10.5	82
	S4	12	9.0	78
	S5	12	10.6	83
Tro 500 mg/kg (28 days)	S6	12	9.7	80
	S7	12	9.6	80
	S8	11	9.1	78
	S9	12	8.2	75
	S10	15	9.5	80
Tro 1000 mg/kg (23 days)	12	15	14.9	92
	13	14	12.3	87
	14	14	14.6	92
	15	15	8.3	76
BSO (14 days)	16	13	10.3	82
	17	13	9.2	79
	18	13	11.6	85
BSO + Tro 1000 mg/kg (14 days)	19	13	8.7	77
	20	13	10.3	82
	21	13	9.2	79

RI, replacement index.

Table 2
Sequence of primers for real-time RT-PCR analyses.

Primer	Sequence
CYP2C8 S[a]	5′-AGATCAGAATTTCTCACCC-3′
CYP2C8 AS[a]	5′-AACTTCGTGTAAGAGCAACA-3′
CYP3A4 S[a]	5′-CCAAGCTATGCTCTTCACCG-3′
CYP3A4 AS[a]	5′-TCAGGTCCACTTACGGTGC-3′
SULT1A1 S	5′-ATGGAGACTCTGAAAGACACACCGG-3′
SULT1A1 AS	5′-TGTGCTGAACCACGAAGTCCACG-3′
UGT1A1 S[b]	5′-CCTTGCCTCAGAATTCCTTC-3′
UGT1A1 AS[b]	5′-ATTGATCCCAAAGAGAAAACCAC-3′
GAPDH S[a]	5′-CCAGGGCTTTTAACTC-3′
GAPDH AS[a]	5′-GCTCCCCCCTGCAAATGA-3′

S, sense primer; AS, antisense primer.
[a] From Katoh et al. (2004).
[b] From Izukawa et al. (2009).

2.10. CYP2C8 and CYP3A4 activities

Liver microsomes from the chimeric or control mice were prepared as described previously (Katoh et al., 2004) and stored at −80 °C until analysis. The protein concentration was determined using Bradford assay reagent (Bio-Rad, Hercules, CA) with bovine γ globulin as the standard. The typical incubation mixtures (total volume, 0.2 ml) consisted of microsomes in 100 mM potassium phosphate buffer (pH 7.4) containing an NADPH-generating system (0.5 mM $NADP^+$, 5 mM glucose 6-phosphate, 5 mM $MgCl_2$, and 1 unit/ml glucose-6-phosphate dehydrogenase) and a substrate.

Paclitaxel 6α-hydroxylase activity was determined by the method of Willey et al. (1993), with slight modifications. The concentrations of the microsomes and paclitaxel were 0.5 mg/ml and 20 μM, respectively. The reaction mixture was incubated at 37 °C for 10 min, and terminated by adding 1.0 ml of dichloromethane. Testosterone (10 μl of 100 μM) was added as an internal standard. After centrifugation at 900 × *g* for 10 min, the organic phase (500 μl) was evaporated under a gentle stream of nitrogen at 40 °C. The residue was redissolved in 200 μl of mobile phase and then 100-μl portion of the sample was subjected to high-performance liquid chromatography (HPLC). The product formation was determined with a Mightysil RP-8 C8 GP column (5-μm particle size, 4.6 i.d. × 150 mm; Kanto Chemical, Tokyo, Japan). The mobile phase (45% acetonitrile/20 mM ammonium acetate) was used under isocratic condition. The flow rate was 1.0 ml/min, and the column temperature was 35 °C. The eluent was monitored at 227 nm. The quantification of 6α-hydroxypaclitaxel was performed by comparing the HPLC peak heights to that of authentic standards with reference to an internal standard. The retention time of 6α-hydroxypaclitaxel and paclitaxel was 9.0 and 14.7 min, respectively.

The dexamethasone 6-hydroxylase activity was determined according to the method of Tomlinson et al. (1997), with slight modifications. The concentrations of microsomes and dexamethasone were 1.0 mg/ml and 100 μM, respectively. The reaction mixture (total volume, 0.2 ml) was incubated at 37 °C for 30 min, and terminated by adding 1.5 ml of ice-cold ethyl acetate. 6-Hydroxytestosterone (10 μl of 10 ng/μl) was added as an internal standard. After centrifugation at 900 × *g* for 10 min, the organic phase (500 μl) was evaporated under a gentle stream of nitrogen at 40 °C. The residue was redissolved in 200 μl of mobile phase and then 100-μl portion of the sample was subjected to HPLC. The product formation was determined with a Mightysil RP-8 C8 GP column (5-μm particle size, 4.6 i.d. × 150 mm; Kanto Chemical). The mobile phase (23% acetonitrile/0.015% formic acid) was used under isocratic condition. The flow rate was 1.0 ml/min, and the column temperature was 35 °C. The eluent was monitored at 243 nm. The dexamethasone 6-hydroxylase activity was quantified using a standard curve of dexamethasone because we could not obtain pure 6-hydroxydexamethasone. The retention time of 6-hydroxydexamethasone was confirmed using the incubation product of recombinant CYP3A4 and dexamethasone. The retention time of 6-hydroxydexamethasone and dexamethasone was 4.8 and 37.7 min respectively. The final concentration of the solvent in the incubation mixture was less than 1%.

2.11. Statistical analysis

Statistical analyses between multiple groups were performed using one-way analysis of variance (ANOVA), followed by Dunnett's *post hoc* test. Comparisons between two groups were performed using two-tailed Student's *t*-test. A value of $P < 0.05$ was considered statistically significant.

Table 3
Serum biochemical parameters in toroglitazone and/or BSO-administered chimeric mice.

Group	Mouse no.	ALT (U/l)			AST (U/l)		LDH (U/l)		T-Bil (mg/dl)		D-Bil (mg/dl)	
		Initial	Final		Final		Final		Final		Final	
Control	1	108	77		147		1366		0.8		0.1	
	2	90	56		83		2884		0.7		0.1	
	3	140	139		212		1386		0.8		0.1	
	4	87	137		152		1554		0.8		ND	
	5	88	79		126		832		0.9		ND	
	6	92	106		188		1122		0.8		ND	
	Mean ± SD	101 ± 21	99 ± 34	[1.0]	151 ± 46	[1.0]	1524 ± 712	[1.0]	0.8 ± 0.1	[1.0]	0.1 ± 0.0	[1.0]
Tro 1000 mg/kg	7	64	67		170		3600		0.9		0.1	
(14 days)	8	96	233	R	345		2520		1.5		0.4	
	9	144	218	R	283		861		1.0		0.1	
	10	79	167	R	188		1724		0.8		0.1	
	11	39	64		145		897		0.9		0.1	
	Mean ± SD	84 ± 39	150 ± 81	[1.5]	226 ± 84	[1.5]	1920 ± 1161	[1.3]	1.0 ± 0.3	[1.3]	0.2 ± 0.1	[2.0]
	R (n = 3)	106 ± 34	206 ± 35**	[2.1]	272 ± 79	[1.8]	1702 ± 830	[1.1]	1.1 ± 0.4	[1.4]	0.2 ± 0.2	[2.0]
Tro 250 mg/kg	S1	62	344	R	361		2256		0.9		ND	
(28 days)	S2	71	182		250		902		0.9		ND	
	S3	75	70		165		1498		0.7		ND	
	S4	59	146	R	186		823		0.8		ND	
	S5	80	111		130		667		0.8		ND	
	Mean ± SD	69 ± 9	171 ± 105	[1.7]	218 ± 91	[1.4]	1229 ± 655	[0.8]	0.8 ± ±0.1	[1.0]	0.1 ± 0.0	[1.0]
Tro 500 mg/kg	S6	66	108		144		779		0.7		ND	
(28 days)	S7	78	205	R	318		1126		0.7		ND	
	S8	79	48		93		531		0.6		ND	
	S9	81	91		114		487		0.7		ND	
	S10	71	171	R	170		982		0.6		ND	
	Mean ± SD	75 ± 6	125 ± 63	[1.3]	168 ± 89	[1.1]	781 ± 278	[0.5]	0.7 ± 0.1	[0.9]	0.1 ± 0.0	[1.0]
Tro 1000 mg/kg	12	79	504	R	452		1566		0.6		0.1	
(23 days)	13	70	221	R	260		1550		0.7		0.1	
	14	84	345	R	410		1274		0.7		0.1	
	15	113	97		138		729		0.7		ND	
	Mean ± SD	87 ± 19	292 ± 174	[2.9]	315 ± 144	[2.1]	1280 ± 391	[0.8]	0.7 ± 0.1	[0.9]	0.1 ± 0.0	[1.0]
	R (n = 3)	78 ± 7	357 ± 142**	[3.6]	374 ± 101**	[2.5]	1463 ± 164	[1.0]	0.7 ± 0.1	[0.9]	0.1 ± 0.0	[1.0]
BSO	16	58	51		102		1728		0.8		0.2	
(14 days)	17	65	91		131		1206		0.6		0.1	
	18	53	38		123		1504		0.7		0.1	
	Mean ± SD	59 ± 6	60 ± 28	[0.6]	119 ± 15	[0.8]	1479 ± 262	[1.0]	0.7 ± 0.1	[0.9]	0.1 ± 0.1	[1.0]
BSO + Tro	19	117	59		175		1572		0.7		0.2	
1000 mg/kg	20	55	55		105		891		0.6		ND	
(14 days)	21	76	39		144		836		0.8		0.1	
	Mean ± SD	83 ± 32	51 ± 11	[0.5]	141 ± 35	[0.9]	1100 ± 410	[0.7]	0.7 ± 0.1	[0.9]	0.2 ± 0.1	[2.0]

Each parameter except initial value was measured 24 h after the last troglitazone administration.
Differences compared to the control group were considered significant at **$P < 0.01$.
ND, not detected; R, responder; score in parenthesis, ratio to the control.

3. Results

3.1. TRO caused liver injury in chimeric mice with a humanized liver

TRO was orally administered to female chimeric mice at a dose of 250 mg/kg/day for 28 days (Tro 250-28 day), 500 mg/kg/day for 28 days (Tro 500-28 day), and 1000 mg/kg/day for 14 days (Tro 1000-14 day) or 23 days (Tro 1000-23 day) in a non-fasting condition. BSO (10 mM in drinking water) was treated alone or with Tro administration for 14 days. The initial serum ALT levels ranged from 39 to 144 U/l among all animals (Table 3). The final ALT levels in the Tro 250-28 day (171 ± 105 U/l), Tro 500-28 day (125 ± 63 U/l), Tro 1000-14 day (150 ± 81 U/l) and Tro 1000-23 day (292 ± 174 U/l) groups increased by 1.7-, 1.3-, 1.5- and 2.9-fold, respectively compared to the control group (99 ± 34 U/l). Two out of five mice in both Tro 250-28 day and Tro 500-28 day groups, three out of five mice in the Tro 1000-14 day group and three out of four mice in the Tro 1000-23 day group showed increased ALT levels of more than 144 U/l, the highest initial ALT level among all mice. These mice were termed responders (R) in Table 3. The average values of ALT levels in Tro 250-28 day and Tro 500-28 day groups are a little higher than the control group, however there is no clear dose–response in these values. These results suggest that the dose level of 1000 mg/kg is required for the onset of troglitazone-induced liver injury in the chimeric mice. Therefore, we put focus on the results from 1000 mg/kg dose groups in the subsequent analyses. The final ALT levels in responders in the Tro 1000-14 day and Tro 1000-23 day groups were significantly higher than those in the control group by 2.1- and 3.6-fold, respectively (Fig. 1). For the subsequent analyses, the data from the responders (R) in Tro 1000-14 day and Tro 1000-23 day groups were compared to those in the control group.

The final AST level in the Tro 1000-23 day group was significantly higher than that in the control group by 2.5-fold. The final serum LDH, T-Bil and D-Bil levels in the Tro 1000-14 day and Tro 1000-23 day groups were unchanged compared to the control group (Table 3). The LDH, T-Bil and D-Bil levels in the Tro 1000-23 day group were lower than those in the Tro 1000-14 day group. Both in the BSO alone and BSO- and Tro-administered groups, serum ALT, AST, LDH, T-Bil and D-Bil levels were unchanged compared to the levels in the control group (Table 3 and Fig. 1).

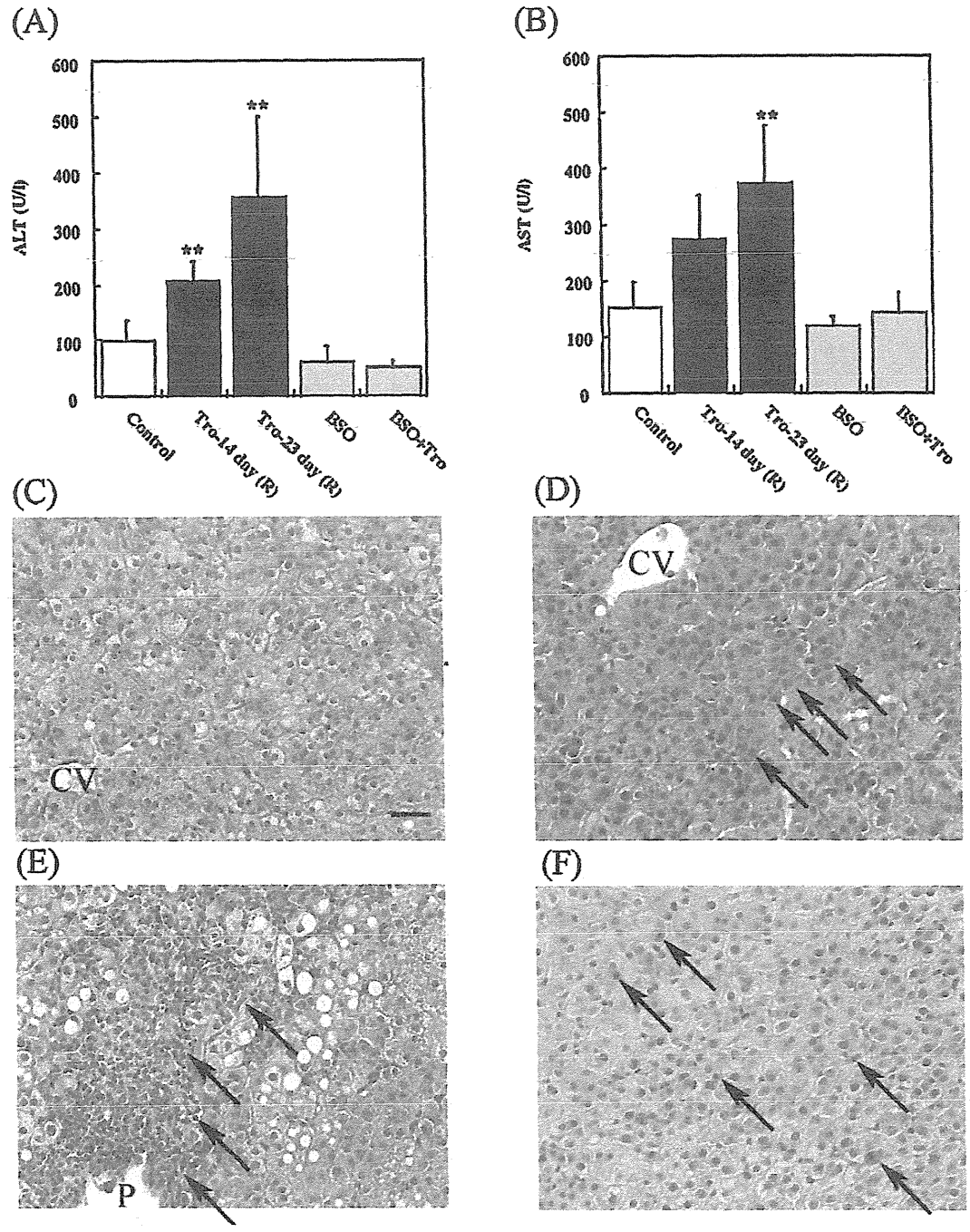

Fig. 1. Changes in the serum ALT and AST levels and liver histology by Tro and/or BSO administration in chimeric mice. The chimeric mice were orally administered Tro (1000 mg/kg/10 ml, suspended in 0.5% CMC) once daily for 14 or 23 days in a non-fasting condition, and 0.5% CMC was administered once daily for 14 days as a control. BSO (10 mM in drinking water) was also given alone or with Tro administration for 14 days. (A) ALT and (B) AST were measured 24 h after the last administration. The data are shown as the mean ± SD of the results from 3 to 6 mice. In the Tro-14 day ($n = 3$) and Tro-23 day ($n = 3$) group, the data are from the responder chimeric mice (R). The differences compared to the control group ($n = 6$) were considered significant at $^{**}P < 0.01$. (C–F) The liver specimens from the chimeric mice were sampled 24 h after the last Tro administration and subsequently stained with H&E. The human hepatocytes in the control chimeric mouse had a clear cytoplasm and no cellular infiltration (C, mouse no. 2). The arrows indicate an eosinophilic change of human hepatocytes (D, mouse no. 12, Responder), neutrophil infiltration (E, mouse no. 13, Responder) and necrosis of human hepatocytes (F, mouse no. 14, Responder). CV: central vein; P: portal vein; Bars: 40 μm (C–F are the same scale).

In the control chimeric mouse, a clear cytoplasm and no cellular infiltration were observed in the human hepatocytes in the liver tissue of the chimeric mice (Fig. 1C). In the responder chimeric mice, the human hepatocytes in the liver tissue showed slight eosinophilic changes (Fig. 1D), neutrophil infiltration surrounding the area of the portal vein (Fig. 1E) and scattered single cell necrosis (Fig. 1F) after Tro administration.

3.2. *Oxidative stress responses in chimeric mice with a humanized liver*

In both the Tro 1000-14 day and Tro 1000-23 day groups, the hepatic GSH contents were significantly higher in the Tro-administered responder mice by approximately 2-fold than in the control group (Fig. 2A). GST activities, SOD2 activities and the

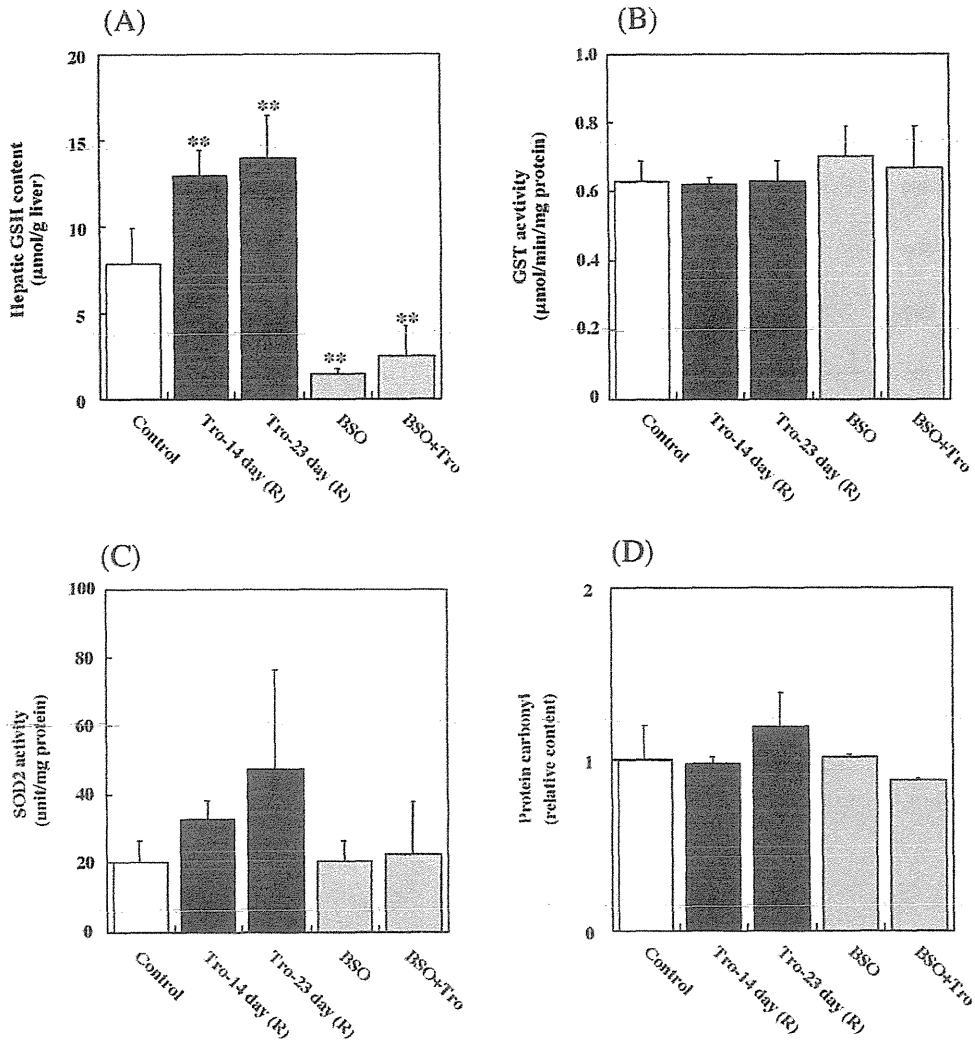

Fig. 2. Changes in the hepatic GSH content (A), GST activity (B), SOD2 activity (C), and plasma protein carbonyl content (D) in the chimeric mice that were administered Tro and/or BSO. The data are shown as the mean ± SD of the results from 3 to 6 mice. In the Tro-14 day and Tro-23 day groups, the data are from the responder chimeric mice. The differences compared to the control group were considered significant at $^{**}P < 0.01$.

protein carbonyl content showed no significant change following Tro administration (Fig. 2B–D). SOD2 activity in the Tro 1000-23 day group was higher than in the control: however, the difference in activity was not significant.

The effects of the GSH-lowering agent BSO on oxidative stress in the chimeric mice were evaluated. The hepatic GSH contents were significantly decreased in the BSO group by approximately 0.2-fold compared to the control group. However, in the BSO and Tro-administered group, the GSH content was suppressed by Tro administration. The hepatic GST activities were unchanged with the administration of BSO alone or BSO and Tro administration. The administration of BSO and Tro showed no change in SOD2 activity. The protein carbonyl contents also showed no change among the groups in this study (Fig. 2D). These results suggested that Tro induced the GSH synthesis enzyme, which was inhibited by BSO.

3.3. *Effect of Tro and/or BSO administration on the expression of drug metabolizing enzymes in the chimeric mice with a humanized liver*

We determined the expression levels of drug metabolizing enzymes, which are involved in the metabolism of Tro in human. The expression level of human CYP2C8 mRNA (Fig. 3A) was increased with the administration of Tro and/or BSO. The expression level of CYP2C8 protein (Fig. 3B) and paclitaxel 6a-hydroxylase activities (Fig. 3C) were significantly increased by the administration of Tro. The expression levels of CYP3A4 mRNA (Fig. 4A) and protein (Fig. 4B) also tended to increase with the administration of Tro and/or BSO. Dexamethasone 6-hydroxylase activities were significantly increased by the administration of Tro and/or BSO. Therefore, these results clearly demonstrated that Tro induced CYP2C8 and CYP3A4 in the liver of the chimeric mice with a humanized liver. Interestingly, the administration of BSO alone also induced both enzymes. Based on these data, enzyme induction is unlikely to be involved in Tro-induced liver injury. In addition, we found that Tro induced the expression level of human UGT1A1 (Fig. 5B) mRNA. The administration of BSO and/or Tro also induced the expression level of UGT1A1 mRNA.

4. Discussion

During the preclinical development and following the withdrawal of Tro, pharmaceutical companies performed numerous toxicity studies using mice, rats and monkeys (Watanabe et al.,

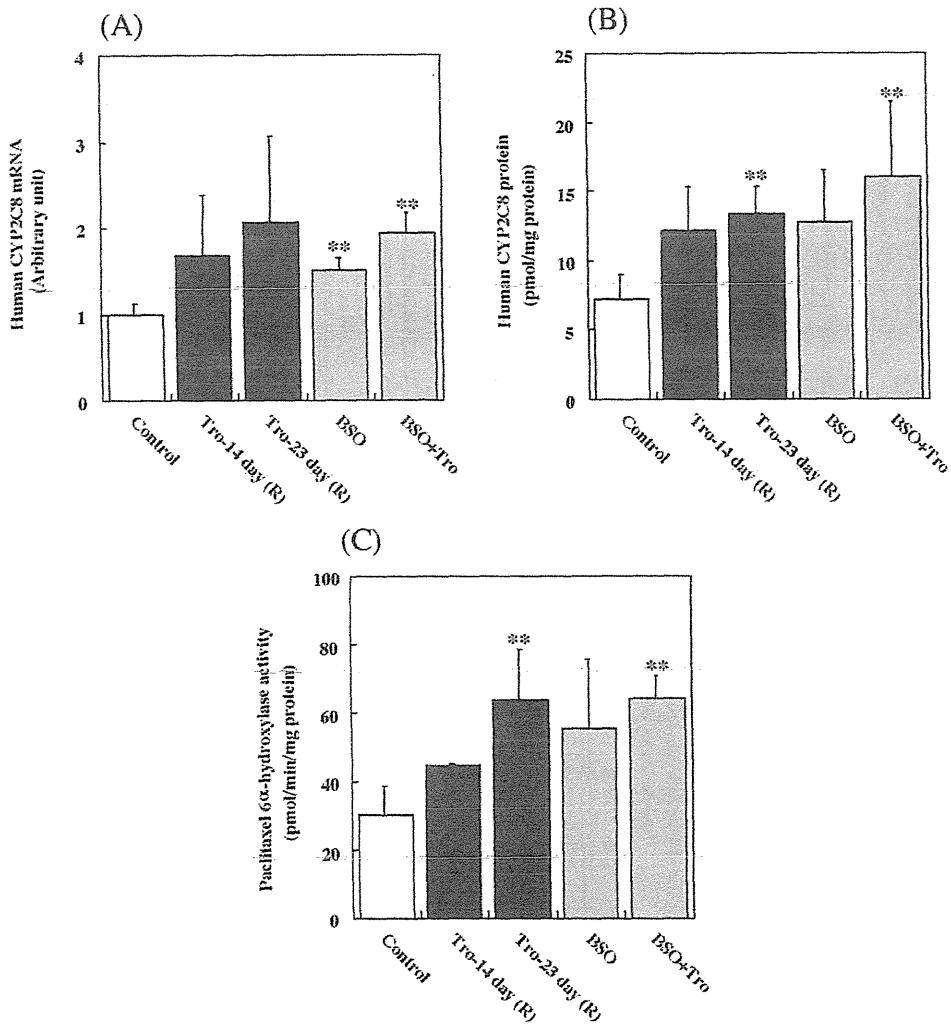

Fig. 3. Changes in the expression level of human CYP2C8 mRNA (A), protein content (B), and enzyme activity (C) in the liver of chimeric mice that were administered Tro and/or BSO. Paclitaxel 6a-hydroxylase activity was catalyzed by CYP2C8 and measured using 20 μM paclitaxel as a substrate. The data are shown as the mean ± SD of the results from 3 to 6 mice. In the Tro-14 day and Tro-23 day groups, the data are from the responder chimeric mice. The differences compared to the control group were considered significant at $^{**}P < 0.01$.

1999). In these toxicity studies, Tro was administered at a dose of 800 mg/kg/day for 24 months to mice, 1200 mg/kg/day for 12 months to rats and 1200 mg/kg/day for 12 months to monkeys, but no signs of liver dysfunction were confirmed (Watanabe et al., 1999). Chimeric mice with a humanized liver are suitable for *in vivo* studies utilizing human hepatocytes. The present study used chimeric mice with a humanized liver and successfully demonstrated Tro-induced liver with the once daily oral administration for 14 and 23 days of 1000 mg/kg Tro. The development of Tro-induced liver injuries in the responder chimeric mice was confirmed by the significant increase in the final serum ALT and AST levels that occurred in an administration-duration-dependent manner (Fig. 1A and B), the eosinophilic changes (Fig. 1D) and cellular infiltrations in the liver tissue (Fig. 1E) and single cell necrosis of human hepatocytes (Fig. 1F). Using the same chimeric mice, Schulz-Utermoehl et al. (2012) did not demonstrate liver injury administering a once daily oral dose for 7 days of 300 and 600 mg/kg Tro, and no significant differences in the pharmacokinetics parameters of C_{max} or AUC were observed following doses of Tro at 300 and 600 mg/kg. These evidences support our results that 250 and 500 mg/kg of Tro was insufficient for the onset of Tro-induced liver injury in the chimeric mice when dosed once daily for 28 days. Both the dose level and the dosing period will be essential factors for the onset of Tro-induced liver injury.

The increase of serum transaminases was considered to be derived from the human hepatocytes, which was supported by the histological changes. However, we were unable to distinguish human ALT from mouse ALT quantitatively (data not shown). Conversely, two out of five mice in the Tro 1000-14 day group and one out of four mice in the Tro 1000-23 day group did not show hepatic injury. As shown in Table 1, the chimeric mice exhibited a hAlb concentration of 8.0–14.9 mg/ml and 75–92% of RI and received transplanted human hepatocytes from the same donor. The hAlb levels of the non-responder chimeric mice ranged from 8.2 (RI: 75%) to 11.7 mg/ml (RI; 85%), and appeared to not be critically different from the hAlb levels of the responder chimeric mice, which ranged from 9.0 (RI: 78%) to 14.9 (RI: 92%). Therefore, it was considered that the individual difference in the onset of liver injury among the mice would depend on other factors as discussed below.

It has been reported that the double null mutant of GSTT1 and GSTM1 in humans correlated with Tro-associated abnormal increases in ALT levels (odds ratio, 3.692; 95% confidence interval, 1.354–10.066; $P = 0.008$) (I. Watanabe et al., 2003). However, the present study revealed that the difference in the onset of liver injury

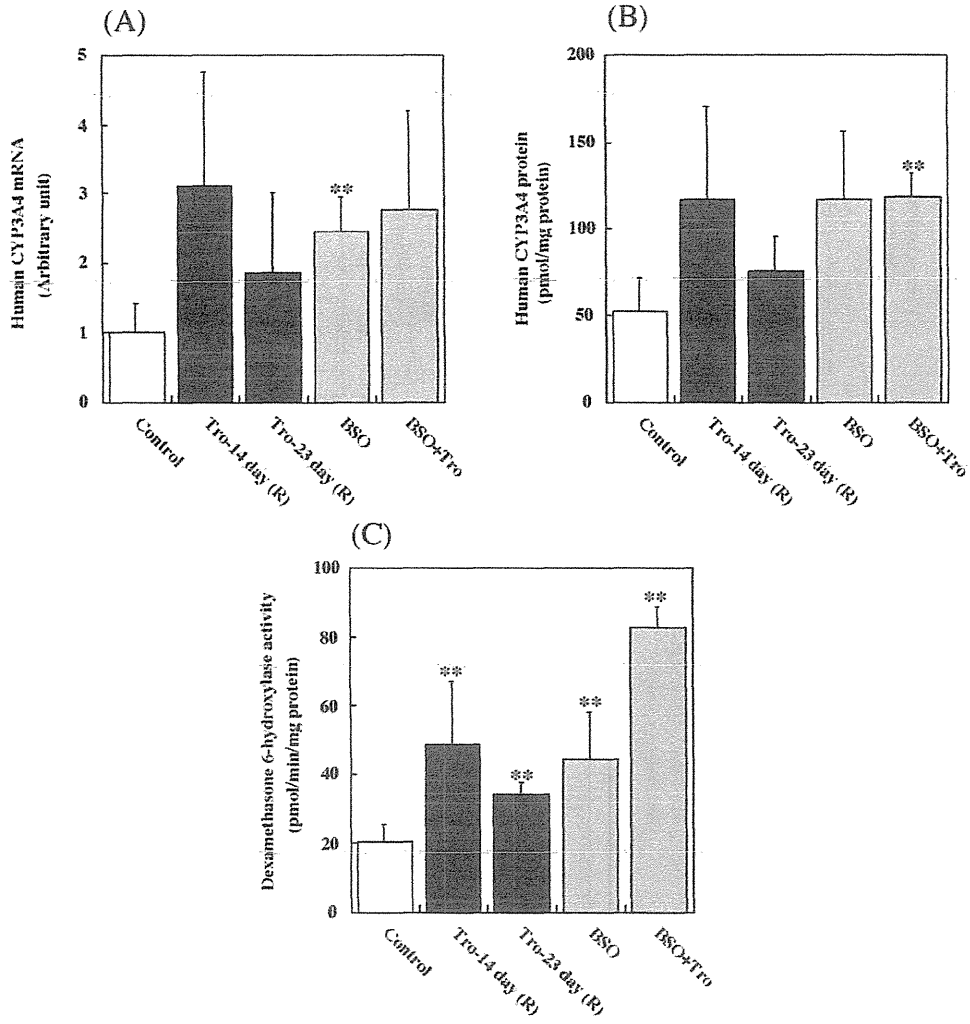

Fig. 4. Changes in the expression level of human CYP3A4 mRNA (A), protein content (B), and enzyme activity (C) in the liver of chimeric mice administered Tro and/or BSO. Dexamethasone 6-hydroxylase activity was catalyzed by CYP3A4 and measured using 100 μM dexamethasone as a substrate. The data are shown as the mean ± SD of the results from 3 to 6 mice. In the Tro-14 day and Tro-23 day groups, the data are from the responder chimeric mice. The differences compared to the control group were considered significant at $^{**}P < 0.01$.

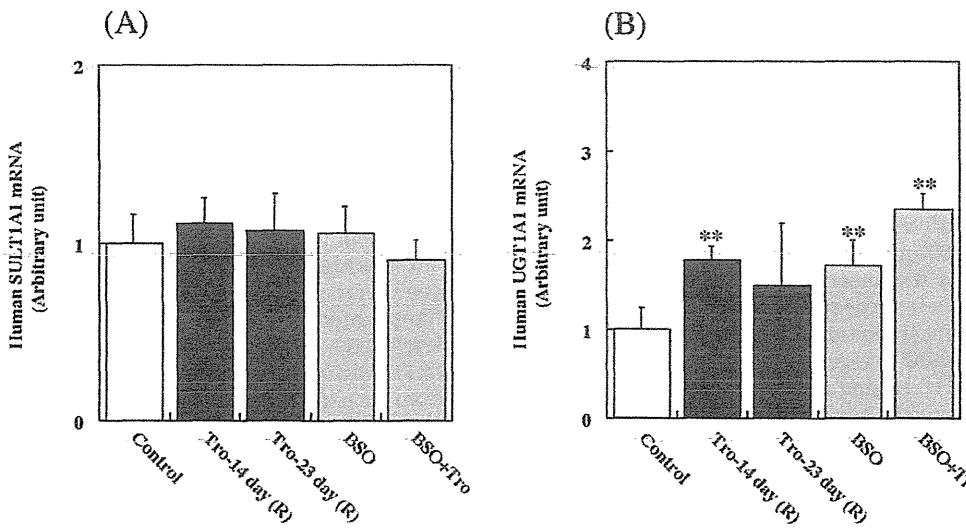

Fig. 5. Changes in the expression level of human SULT1A1 mRNA (A) and human UGT1A1 mRNA expression (B) in the liver of chimeric mice that were administered Tro and/or BSO. The data are shown as the mean ± SD of the results from 3 to 6 mice. In the Tro-14 day and Tro-23 day groups, the data are from the responder chimeric mice. The differences compared to the control group were considered significant at $^{**}P < 0.01$.

could be Tro-induced in the chimeric mice with genetically identical human hepatocytes genotyped to wild-type GSTT1 and GSTM1 (data not shown). It is conceivable that the double null mutant of GSTT1 and GSTM1 is unlikely to be a risk factor, which was recently suggested by Usui et al. (2011) using cytotoxicity assays of human hepatocytes.

BSO was administered to evaluate the effects of GSH depletion on Tro-induced liver injury. The suspected active metabolite of Tro, a quinone metabolite, has been reported to not react directly with GSH, and it can be further metabolized to an O-quinone methide or undergo ring opening to produce additional highly electrophilic intermediates (Kassahun et al., 2001). However, in this study, neither the serum biochemical analyses nor the histological examinations showed evidence of liver injury in the BSO alone and BSO- and Tro-administered group, whereas the hepatic GSH contents decreased approximately 0.2- and 0.4-fold in these groups, respectively compared to the control group (Fig. 2A). Furthermore, hepatic GST activities were maintained in all groups (Fig. 2B). Although the results in this study appear to not support the general understanding of scavenging systems for reactive metabolites, it was suggested that the onset of Tro-induced liver injury was independent of scavenging systems associated with hepatic GSH. Interestingly, the hepatic GSH contents significantly increased with the administration of Tro (Fig. 2A), although the functional mechanism in relation to the onset of liver injury was unclear.

SOD2 activity and protein carbonyl contents were measured to clarify whether an increase in oxidative stress might be associated with the onset of Tro-induced liver injury (Fig. 2C and D), as reported in a study using *SOD2*$^{+/-}$ mice (Ong et al., 2007). In the *SOD2*$^{+/-}$ mouse study, the increase in the serum AST level and the degeneration of hepatocytes were observed when 30 mg/kg of Tro was intraperitoneally administered once per day for 4 weeks (Ong et al., 2007). However, the phenomenon was not reproduced by other group (Fujimoto et al., 2009) despite the administered to the same dose to the same *SOD2*$^{+/-}$ mice. We found that SOD2 activities were tended to increase in the Tro-23 day group. Furthermore, the protein carbonyl contents were unchanged. These results suggest that oxidative stress may not involved in Tro-induced liver injury in the chimeric mice.

In humans, Tro is metabolized by three pathways, *i.e.*, sulfation by SULT1A1 (Honma et al., 2002), glucuronidation by UGT1A1 (Yoshigae et al., 2000), and oxidation to form a quinone metabolite (M3) by CYP2C8 and CYP3A4 (Yamazaki et al., 1999; Yamamoto et al., 2002). Recently, the chimeric mice were confirmed to show the unique profiles in metabolism of Tro when compared to SCID mice (Schulz-Utermoehl et al., 2012). A total of 32 putative metabolites plus Tro were detected in blood from the chimeric mice, with 14 (M1, M4–M10, M12 and M17–M21) of these metabolites detected only in blood from the chimeric mice. Of these 14 metabolites, 4 (M4, M7, M8 and M12) were also detected only in liver extracts from the chimeric mice. The relative concentrations of the glucuronide metabolite (M13) were higher in liver preparations from SCID mice. These findings suggested the chimeric mice possess metabolically active human hepatocytes and have a potential to generate unique human metabolite (Schulz-Utermoehl et al., 2012). The involvement of a sulfo-conjugate in Tro-induced liver injury was suggested in *in vitro* study by Saha et al. (2010) who reported that a sulfo-conjugate of Tro exerted direct toxic effects on human hepatocytes, possibly *via* oxidative stress induction. In contract, the expression level of SULT1A1 mRNA was not changed in this study, suggesting the difference effect of Tro between *in vivo* and *in vitro* study.

We found that CYP2C8 and CYP3A4 were induced by the administration of Tro, as previously reported (Sahi et al., 2003). However, the onset of the Tro-induced liver injury was considered independent of the induction of these drug-metabolizing enzymes because enzyme induction was also observed in the BSO alone- and BSO and Tro-administered group. The cause of the moderate induction of CYP3A4 in the Tro-23 day group compared with the Tro-14 day group remains unclear. However, it was reported that hepatic expression levels of proinflammatory cytokines, tumor necrosis factor (TNF) α and interleukin (IL)-6 and chemokines were increased in the mouse model of drug-induced liver injury (Toyoda et al., 2011, 2012). TNFα was also identified to be involved in the down-regulation of CYP3A11 and CYP3A25 in mouse liver (Kinloch et al., 2011). In addition, IL-6 was reported to down-regulate the expression of CYP3A4 *via* pregnane X receptor in human hepatocytes (Yang et al., 2010). Taking these recent reports into consideration, chronic hepatic inflammation in the Tro-23 day group might be a causal factor for the decreased expression level of CYP3A4 in this study.

As shown in Fig. 5B, UGT1A1 appears unrelated to the onset of the Tro-induced liver injury because significant increases in human UGT1A1 mRNA expression were observed not only in the Tro-14 day group but also in the BSO alone and BSO- and Tro-administered groups.

Notably, the chimeric mice were generated using an uPA$^{+/+}$/SCID mouse line, which is defective in functional T and B lymphocytes (Bosma et al., 1983). Tro-induced liver injury in the chimeric mice could be successfully produced when free from T and B lymphocyte-mediated immune responses. However, SCID mice were once daily orally administered Tro at 300 and 600 mg/kg doses for 7 days and showed no change in ALT and AST levels (Schulz-Utermoehl et al., 2012). Further investigations comparing SCID mice and the chimeric mice with a humanized liver are necessary.

Idiosyncratic liver injury is a critical issue for clinical practice and drug development. Thus, numerous attempts have been made to establish a method for predicting idiosyncratic liver injury in human. The present study succeeded in demonstrating Tro-induced liver injury using chimeric mice with a humanized liver. The advantage of this mouse model is to enable human hepatocytes to be examined in an *in vivo* environment. The chimeric mice with a humanized liver will be a useful tool to investigate the unsolved mechanism of idiosyncratic Tro-induced hepatic injury.

Funding information

Health and Labor Sciences Research Grants from the Ministry of Health, Labor, and Welfare of Japan (H23-BIO-G001).

Conflict of interest statement

The authors declare that there are no conflicts of interest.

References

Bedoucha, M., Atzpodien, E., Boelsterli, U.A., 2001. Diabetic KKAy mice exhibit increased hepatic PPARγ1 gene expression and develop hepatic steatosis upon chronic treatment with antidiabetic thiazolidinediones. Journal of Hepatology 35, 17–23.

Bosma, G.C., Custer, R.P., Bosma, M.J., 1983. A severe combined immunodeficiency mutation in the mouse. Nature 301, 527–530.

Fujimoto, K., Kumagai, K., Ito, K., Arakawa, S., Ando, Y., Oda, S., Yamoto, T., Manabe, S., 2009. Sensitivity of liver injury in heterozygous Sod2 knockout mice treated with troglitazone or acetaminophen. Toxicologic Pathology 37, 193–200.

Habig, W.H., Pabst, M.J., Jakoby, W.B., 1974. Glutathione S-transferases. The first enzymatic step in mercapturic acid formation. Journal of Biological Chemistry 249, 7130–7139.

He, K., Talaat, R.E., Pool, W.F., Reily, M.D., Reed, J.E., Bridges, A.J., Woolf, T.F., 2004. Metabolic activation of troglitazone: identification of a reactive metabolite and mechanisms involved. Drug Metabolism and Disposition: The Biological Fate of Chemicals 32, 639–646.

Honma, W., Shimada, M., Sasano, H., Ozawa, S., Miyata, M., Nagata, K., Ikeda, T., Yamazoe, Y., 2002. Phenol sulfotransferase, ST1A3, as the main enzyme catalyzing sulfation of troglitazone in human liver. Drug Metabolism and Disposition: The Biological Fate of Chemicals 30, 944–949.